Fully Relativistic Band Structure Calculations for Magnetic Solids – Formalism and Application

H. Ebert

Institut für Phys. Chemie, Univ. München, Butenandtstr. 5-13, D-81377 München

Abstract. Relativistic effects, in particular the spin-orbit coupling, give rise for magnetic systems to a great number of interesting and technologically important phenomena. The formal and technical aspects of corresponding fully relativistic theoretical investigations are reviewed. The properties of the underlying Dirac equation, set up within the framework of density functional theory (DFT) are discussed together with the Breit-interaction and Brooks' orbital polarization mechanism. As an example for a corresponding band structure method, the Korringa-Kohn-Rostoker (KKR) Green's function method is adopted. In particular, some technical aspects specific to this technique are discussed. The numerous applications that will be presented are primarily meant to demonstrate the many different facets of relativistic – this means in general – of spin-orbit induced effects in magnetic solids. In addition, these also demonstrate the tremendous flexibility of band structure schemes based on the Green's function formalism.

1 Introduction

Relativistic influences on the electronic properties of solids are known for quite a long time. One of the most prominent examples for these is the position of the optical absorption edge of Au. Compared to that of Ag this is higher in energy giving rise to the characteristic yellow colour of Au [1]. Another example is the relativistic contraction of s-type electronic shells, that has important consequences even in chemistry [2]. In the case of Au this leads to the existence of Au^--ions in the compounds CsAu and RbAu, while corresponding Ag-compounds are not found. One of the early hints for the importance of spin-orbit coupling for the electronic band structure of solids stems from X-ray absorption experiments. Namely, it was observed by Cauchois and Manescu [3] that for the L_3-absorption spectrum of Pt there occurs a *white line* at the absorption edge while none was found for the L_2-edge. Mott [4] ascribed this finding to the spin-orbit coupling, that should cause the d-states of Pt above the Fermi-energy to have predominantly $d_{5/2}$-character. As a consequence of this and because of the dipole selection rules $\Delta j = 0, \pm 1$ on expects strong absorption for the L_3-edge but not for the L_2-edge. Another example for the influence of the spin-orbit coupling is supplied by de Haas-van Alphen-experiments on W. Here it was found that the electron- and hole-surfaces do not touch in the Γ-H-direction, as it was predicted from non-relativistic band structure calculations [5]. The mentioned experiments and many others clearly demonstrated the influence of relativistic effects and that way the need to account for them within a corresponding band

H. Dreyssé (Ed.): Workshop 1998, LNP 535, pp. 191–246, 1999.

structure calculation. Nevertheless, it will in general depend on the specific experiment one wants to describe to what extent this has to be done. For example, in the case of the quadrupolar and magnetic hyperfine interaction, that takes place in the vicinity of the nucleus where relativistic influences on the electrons are most pronounced, these will show up even for relatively light elements [6].

For many cases, it is well justified to deal with relativistic effects by introducing corresponding corrections to the Schrödinger equation. One of the standard techniques to derive these is to apply a Foldy-Wouthuysen-transformation to remove the coupling between the large and small component of the Dirac equation [7]. Because of technical problems connected with this approach – in particular its convergence behavior – several alternative schemes have been suggested that in general also lead to a two-component formalism and that in some cases are also somewhat problematic. Among these for example the elimination methods [8–14], the Douglas-Kroll-Heß-transformation [15], or the ZORA-scheme [16] aim to derive an effective Hamiltonian that contains – compared to a non-relativistic Schrödinger-Hamiltonian – relativistic correction terms. In contrast to this, Gesztesy et al. worked out an expansion scheme for the corresponding Green's function [17,18]. In spite of the obvious differences between the various schemes mentioned, they nevertheless all lead to the mass-velocity, the Darwin and the spin-orbit coupling terms [7] as the most important corrections, that are all proportional to $(1/c^2)$. Of course, the explicit expressions supplied by the various approaches differ to some extent. Nevertheless, one may unambiguously call the first two correction terms scalar-relativistic because of their transformation properties [19]. Most important, these imply that the scalar-relativistic corrections leave spin as a good quantum number. Accordingly, it is very simple to include them in a band structure programme that is set up in a non-relativistic way - even for spin-polarized systems. However, one has to note that modifying the basic electronic Hamiltonian, one may have to adopt the expressions for operators representing physical observables [20,21]. The most prominent example is that for the Fermi-contact part of the magnetic hyperfine interaction. Inconsistent scalar-relativistic calculations indicated for example for 3d-transition metals relativistic corrections in the order of 40 % [22,23] while these amount only to about 10 % [24,25]. Another important example in this context is the electron-photon interaction operator. While this implies the selection rule $\Delta m_s = 0$ for the non-relativistic case, the corresponding relativistic corrections involve the spin-orbit coupling operator allowing for that reason for spin-flip optical transitions [21,26–28].

Compared to the scalar-relativistic corrections, accounting for the spin-orbit coupling within a band structure calculation is much more demanding because the corresponding correction operator contains explicitly the spin operator. An efficient way to include its effects within a band structure calculation, that is based on the variational principle, is to add the matrix of the corresponding operator to the Hamiltonian matrix in the secular equation [29,30]. For a paramagnetic system this will increase the time to solve the secular equation by a factor of 8 because the dimension of the matrices is doubled. This computa-

tional effort can be reduced to some extent by applying the second variational technique [31]. Because in both cases the basis functions are set up only in a non- or scalar-relativistic level, it was often argued that this procedure will lead to problems if the spin-orbit coupling is very strong. However, recently it could be demonstrated that one can apply it without problems even to compounds containing Pb, for which the spin-orbit coupling for the p-states is quite high [32]. Of course, the most reliable way to deal with all relativistic effects is to start from the Dirac equation. In fact, for more or less any of the standard band structure methods corresponding versions have been developed during the last 30 years (for example APW [33], OPW [34], KKR [35,36], ASW [37]). Dealing with paramagnetic solids these methods do not require more computer time than accounting for spin-orbit coupling in the variational step, because the dimension of the Hamiltonian matrix is just the same. In spite of this, the later approach seems to be much more popular because it allows one to discuss the final results in familiar terms.

In contrast to the scalar-relativistic corrections, the spin-orbit coupling has many far-reaching consequences for the qualitative aspects of the electronic structure. The reason for this is the lowering in symmetry that is caused by the coupling of the spin and orbital degrees of freedom, that leads – among others – to a removal of energetic degeneracies. Another consequence of spin-orbit coupling is the occurrence of physical phenomena, that cannot be described within a non- or scalar-relativistic framework. A very well-known example for this is the so-called Fano-effect [38,39], that denotes the finding that one obtains a spin-polarized photo-electron current even for a paramagnetic solid [40] if one uses circularly polarized light. Of course, the spin polarization gets just reversed if the helicity of the radiation is reversed. For a magnetic solid, however, this symmetry is broken. A direct consequence of this broken symmetry are the magneto-optical Kerr-effect [41,42] in the visible regime of light and the circular magnetic X-ray dichroism [42,43] at higher photon energies. Of course, there are many other phenomena in magnetic solids, that are caused by the common occurrence of spin-orbit coupling and spin-polarization, as for example the galvano-magnetic phenomena [44], the magneto-crystalline anisotropy [45], orbital contributions to the hyperfine fields and magnetic moments [24] or electric field gradients in cubic solids [46].

The first band structure calculations aiming to calculate spin-orbit induced properties in magnetic solids have been done by Callaway and coworkers [29,26,47]. These authors and later on many other authors [48–56] accounted for spin-orbit coupling in the variational step with the unperturbed Hamilton matrix describing a spin-polarized system. The basis functions used in this approach depend only on the orbital angular momentum quantum number l but carry no information on the spin-orbit coupling. This does not apply to the scheme suggested by the author [57] for which the role of the exchange splitting and the spin-orbit coupling are interchanged compared to the approach of Callaway and others. In particular this means that four-component basis functions are used that are obtained as solutions to the Dirac equation for a spin-averaged poten-

tial, while the spin-dependent part is accounted for in the variational step. An alternative way to include the influence of spin-orbit coupling already in the wave functions has been used by McLaren and Victora [58]. These authors adopted the formalism suggested by Koellling and Harmon [10] that works with two component wave functions in a (l, m_l, m_s)-representation and that leads to coupled sets of radial differential equations if the spin-orbit coupling term is included. A very similar scheme has been used by Akai [59], who restricted the effect of the spin-orbit coupling to within a spin subsystem keeping spin as a good quantum number that way. To avoid the numerical effort in solving the coupled set of radial differential equations, Ankudinov [60] suggested an approximate scheme that is exact for vanishing spin-orbit coupling or vanishing exchange splitting and interpolates between these two extreme cases. Because the later three schemes account for spin-orbit coupling and exchange splitting already in calculating the wave functions, they can be used straightforwardly as a starting point for multiple scattering theory.

To deal with all relativistic effects and magnetism – at least for transition metals this means first of all spin polarization – on the same level, it was suggested already in the 1970s to work on the basis of the appropriate Dirac equation. Dealing with exchange and correlation within the framework of density functional theory this leads in a rather natural way to current density functional theory (CDFT) [61] instead of the conventional spin density functional theory (SDFT) [62]. However, because of the many unsolved problems connected with this general scheme a relativistic version of spin density functional theory has been suggested [63,64]. Instead of dealing with the resulting Dirac-Hamiltonian for spin-polarized systems, Richter and Eschrig [65] suggested to use the corresponding squared Dirac Hamiltonian and developed a corresponding spin-polarized relativistic LCAO-band structure method. The first step to start from the spin-polarized relativistic Dirac equation itself has been done already 20 years ago by Doniach and Sommers, who derived the corresponding coupled radial Dirac equation [66]. The problem has later been investigated in more detail by Feder et al. [67] and Strange et al. [68]. In particular these authors could present the first numerical solution to the coupled radial equations for a single potential well. With this crucial step done, it is possible to derive for any band structure method its spin-polarized relativistic (SPR) version. This has been done for example for the KKR [67,68], the LMTO [57,69], and the ASW [70] methods.

In the case of the SPR-KKR the $\boldsymbol{k}$-space mode based on the variational principle [71] as well as the multiple scattering mode leading directly to the Green's function [24,67,72] has been generalized accordingly. In particular the later approach (SPR-KKR-GF) was extensively used during the last 10 years. Some reasons for this are that one does not require Bloch symmetry for the investigated system and that one can link it straightforwardly to the Coherent Potential Approximation (CPA) alloy theory [73]. A major drawback of the SPR-KKR is its numerical effort required for complex systems. This problem could be overcome for many situations by the development of a TB-version [74,75] and the use of real space cluster techniques [76–78]. Nearly all SPR-KKR-

GF calculations performed so far were based on a muffin-tin or atomic sphere approximation (ASA) construction of the potential. A full-potential version of it has been worked out by various authors [79–81] and could be implemented recently in a self-consistent way [82,83]. Although in practice sometimes tedious because of the complex wave functions, it is possible to investigate more or less any property of magnetic solids using the SPR-KKR-GF formalism. In particular it is now one of the standard starting points to deal with magnetic dichroism in many kinds of electron spectroscopy as for example in X-ray absorption [84,85], in X-ray fluorescence [86], core-level XPS [87,88], valence band XPS [89], angular resolved valence band UPS [90], magnetic scattering [91], and the Faraday effect in the X-ray regime [92].

Most of the benefits supplied by the SPR-KKR-GF method can also be obtained using a corresponding version of the TB-LMTO-method [93–95]. Thus, it seems for many purposes and situations just a matter of taste which one of the band structure schemes is used. In the following the SPR-KKR-GF is described in some detail and a number of applications is used to demonstrate its great flexibility.

2 Formalism

2.1 Relativistic Density Functional Theory

When dealing with the electronic structure of magnetic solids one usually neglects the influence of orbital magnetism on it. Accordingly, corresponding band structure calculations are in general done on the basis of spin density functional theory (SDFT) as it has been derived among others by von Barth and Hedin [62] in a non-relativistic way. This framework seems still to be acceptable when relativistic effects are included by introducing corresponding corrections terms to the Schrödinger equation. If fully relativistic calculations are performed instead, in principle a corresponding basis should be adopted to deal with many-body effects. The first step in this direction has been done by Rajagopal and Callaway [61], who derived the SDFT starting from a relativistic level. These authors demonstrated in particular that quantum electrodynamics supplies the proper framework for a relativistically consistent density functional theory and derived the corresponding relativistic Kohn-Sham-Dirac equations [96,97]:

$$\left[c\boldsymbol{\alpha}\cdot\left(\frac{\hbar}{\mathrm{i}}\boldsymbol{\nabla}+\frac{e}{c}\boldsymbol{A}_{\mathrm{eff}}(\boldsymbol{r})\right)+\beta mc^2+V_{\mathrm{eff}}(\boldsymbol{r})\right]\Psi_i(\boldsymbol{r})=\epsilon_i\Psi_i(\boldsymbol{r}) \tag{1}$$

with

$$V_{\mathrm{eff}}(\boldsymbol{r}) \;=-e\left[A^0_{\mathrm{ext}}(\boldsymbol{r})+\frac{1}{c}\int d^3r'\,\frac{J^0(\boldsymbol{r}')}{|\boldsymbol{r}-\boldsymbol{r}'|}+c\frac{\partial E_{\mathrm{xc}}[J^\mu]}{\partial J^0(\boldsymbol{r})}\right] \tag{2}$$

$$\boldsymbol{A}_{\mathrm{eff}}(\boldsymbol{r})=-e\left[\boldsymbol{A}_{\mathrm{ext}}(\boldsymbol{r})+\frac{1}{c}\int d^3r'\,\frac{\boldsymbol{J}(\boldsymbol{r}')}{|\boldsymbol{r}-\boldsymbol{r}'|}+c\frac{\partial E_{\mathrm{xc}}[J^\mu]}{\partial \boldsymbol{J}(\boldsymbol{r})}\right]. \tag{3}$$

Here the $\Psi_i(\boldsymbol{r})$ are four-component wave functions (see below) with corresponding single particle energies ϵ_i. The matrices α_i and β are the standard 4×4-Dirac matrices [7]. The effective scalar and vector potentials, V_{eff} and $\boldsymbol{A}_{\text{eff}}$, respectively, contain as a first term the corresponding external contributions. The second terms in Eqs. (2) and (3) are the familiar Hartree potential and the vector potential due to the Breit-interaction, respectively. Finally, the third terms are caused by exchange and correlation with the corresponding exchange and correlation energy $E_{\text{xc}}[J^\mu]$ being a functional of the electronic four-current J^μ. This central quantity that determines all properties of the system is given by:

$$J^0 = -ec \sum_i \Psi_i^\dagger \Psi_i \tag{4}$$

$$J^\mu = -ec \sum_i \Psi_i^\dagger \beta \alpha^\mu \Psi_i \ , \tag{5}$$

where J^0/c is identical with the familiar electronic charge density ρ, while the other components J^μ give the spatial components of the electronic current density $\boldsymbol{j}$.

Thus, in contrast to non-relativistic SDFT, where the central quantities are the spin densities $n^{\uparrow(\downarrow)}$ or equivalently the particle density n and spin magnetization density $\boldsymbol{m}$, the relativistic formalism leads in a natural way to a current density functional theory (CDFT). Because of the problems connected with this very general scheme an approximate relativistic version of SDFT has been worked out by several authors [61,63,98–100]. The first step in this direction is the Gordon decomposition of the spatial current density into its orbital and spin parts [61,97,101]:

$$\boldsymbol{j}_{\text{orb}} = \frac{1}{2m} \Psi^\dagger \beta \left[\frac{1}{\mathrm{i}} \overleftarrow{\boldsymbol{\nabla}} - \frac{1}{\mathrm{i}} \boldsymbol{\nabla} + 2e\boldsymbol{A} \right] \Psi \ + \ \frac{1}{2m} \boldsymbol{\nabla} \times \Psi^\dagger \beta \boldsymbol{\sigma} \Psi \tag{6}$$

where $\boldsymbol{\sigma}$ is the vector of 4×4-Pauli matrices [7]. The coupling of the spin part $\boldsymbol{j}_{\text{spin}}$ (the second term in Eq. (6)) to the vector potential $\boldsymbol{A}_{\text{eff}}$ may alternatively be described by introducing the corresponding spin magnetization density

$$\boldsymbol{m} = -\mu_{\text{B}} \sum_i \Psi_i^\dagger \beta \boldsymbol{\sigma} \Psi_i \ . \tag{7}$$

This leads to the coupling term

$$-\boldsymbol{m} \cdot \boldsymbol{B}_{\text{eff}} \ , \tag{8}$$

with $\boldsymbol{B}_{\text{eff}}$ the effective magnetic field corresponding to $\boldsymbol{A}_{\text{eff}}$. Thus, ignoring the orbital current density contribution $\boldsymbol{j}_{\text{orb}}$ one arrives at a Kohn-Sham-Dirac equation completely analogous to the non-relativistic SDFT Schrödinger equation [97,101]:

$$\left[\frac{\hbar}{\mathrm{i}} c\boldsymbol{\alpha} \cdot \boldsymbol{\nabla} + \beta mc^2 + V_{\text{eff}}(\boldsymbol{r}) + \beta \boldsymbol{\sigma} \cdot \boldsymbol{B}_{\text{eff}}(\boldsymbol{r}) \right] \Psi_i(\boldsymbol{r}) = \epsilon_i \Psi_i(\boldsymbol{r}) \tag{9}$$

with

$$\boldsymbol{B}_{\mathrm{eff}}(\boldsymbol{r}) = \boldsymbol{B}_{\mathrm{ext}}(\boldsymbol{r}) + \frac{\partial E_{\mathrm{xc}}[n, \boldsymbol{m}]}{\partial \boldsymbol{m}(\boldsymbol{r})} \; . \tag{10}$$

This approach has been suggested among others by MacDonald and Vosko [63,98], who justified this simplification by introducing a fictitious magnetic field that couples only to the spin degree of freedom as reflected by Eq. (9). This formal justification has been criticized by Xu et al. [102] because describing a relativistic electronic system in terms of the particle density n and spin magnetization density $\boldsymbol{m}$ alone the magnetic interaction part connected with the electronic current density is not Lorentz invariant. This problem could be circumvented by Rajagopal and coworkers [100,102,103] by considering first the problem for the rest frame of an electron – for which $\boldsymbol{j}_{\mathrm{orb}}$ vanishes – giving a consistent justification for the use of relativistic SDFT.

The orbital current density contribution to E_{xc} – ignored within SDFT – has first been considered by Vignale and Rasolt on a non-relativistic level [104–107]. As one of the central quantities these authors introduce the paramagnetic orbital current density $\boldsymbol{j}_{\mathrm{orb,p}}$ (see below). Because of the restrictions caused by the demand for gauge invariance this is replaced then by the so-called vorticity:

$$\boldsymbol{\nu} = \nabla \times \frac{\boldsymbol{j}_{\mathrm{orb,p}}(\boldsymbol{r})}{n(\boldsymbol{r})} \; . \tag{11}$$

This step in particular allows to derive a local version of non-relativistic CDFT. A corresponding explicit expression for the corresponding E_{xc} has been given for the first time by Vignale and Rasolt [105]:

$$E_{\mathrm{xc}}[n, \boldsymbol{\nu}] = E_{\mathrm{xc}}[n, 0] + \int dx \left(\frac{9\pi}{4}\right)^{1/3} \frac{1}{24\pi^2 r_{\mathrm{s}}} \left(\frac{\chi_{\mathrm{L}}}{\chi_{\mathrm{L}}^0} - 1\right) |\boldsymbol{\nu}(x)|^2 \tag{12}$$

where $r_{\mathrm{s}} = (\frac{3}{4\pi n})^{1/3}$ and

$$\frac{\chi_{\mathrm{L}}}{\chi_{\mathrm{L}}^0} = 1 + 0.02764 r_{\mathrm{s}} \ln r_{\mathrm{s}} + 0.01407 r_{\mathrm{s}} + O(r_{\mathrm{s}}^2 \ln r_{\mathrm{s}}) \tag{13}$$

is the ratio of the diamagnetic susceptibility for the interacting and non-interacting electron gas. Later, more sophisticated expressions for E_{xc} have been given [108].

The Vignale-Rasolt CDFT-formalism can be obtained as the weakly relativistic limit of the fully relativistic SDFT-Dirac equation (1). This property has been exploited to set up a computational scheme that works in the framework of non-relativistic CDFT and accounts for the spin-orbit coupling at the same time [109]. This hybrid scheme deals with the kinematic part of the problem in a fully relativistic way whereas the exchange-correlation potential terms are treated consistently to first order in $1/c$. In particular, the corresponding modified Dirac equation

$$\left[\frac{\hbar}{\mathrm{i}} c\boldsymbol{\alpha} \cdot \boldsymbol{\nabla} + \beta mc^2 + V_{\mathrm{eff}}(\boldsymbol{r}) + \beta \boldsymbol{\sigma} \cdot \boldsymbol{B}_{\mathrm{eff}}(\boldsymbol{r}) + \sum_{\sigma} \beta H_{\mathrm{op},\sigma} P_{\sigma}\right] \Psi_i(\boldsymbol{r}) = \epsilon_i \Psi_i(\boldsymbol{r}) \tag{14}$$

incorporates a term

$$H_{\mathrm{op},\sigma} = -\frac{i\hbar e}{2mc}\left[\boldsymbol{A}_{\mathrm{xc},\sigma}(\boldsymbol{r}), \boldsymbol{\nabla}\right]_+ \ , \tag{15}$$

that explicitly represents the coupling of the orbital current and the exchange-correlation vector potential $\boldsymbol{A}_{\mathrm{xc},\sigma}$. Since in the CDFT-formalism of Vignale and Rasolt $\boldsymbol{A}_{\mathrm{xc},\sigma}$ is defined in a spin-dependent way, the spin-projection operator $P_\sigma = \frac{1\pm\beta\sigma_z}{2}$ appears in addition to $H_{\mathrm{op},\sigma}$ in Eq. (14).

Within the above approximate relativistic CDFT scheme the Breit-interaction has been ignored. This radiative correction accounts for the retardation of the Coulomb-interaction and exchange of transversal photons. A more complete version than that included in Eq. (1) is given by the Hamiltonian [2,110]:

$$\mathcal{H}_{\mathrm{Breit}} = \frac{-e^2}{2R}\boldsymbol{\alpha}_1 \cdot \boldsymbol{\alpha}_2 + \frac{e^2}{2R}\left[\boldsymbol{\alpha}_1 \cdot \boldsymbol{\alpha}_2 - \boldsymbol{\alpha}_1 \cdot \hat{\boldsymbol{R}}\,\boldsymbol{\alpha}_2 \cdot \hat{\boldsymbol{R}}\right] \quad \text{with} \ \ \boldsymbol{R} = \boldsymbol{r}_2 - \boldsymbol{r}_1 \ , \tag{16}$$

where the first part is the magnetic Gaunt part and the second one is the retardation term. While inclusion of the Breit-interaction within quantum-chemical calculations for atoms and molecules is nearly standard [2], so far only one model [111] and one fully relativistic [112] calculation have been done in the case of solids. This is quite astonishing, because the Breit-interaction gives rise to the so-called shape anisotropy, that contributes in general to the magneto-crystalline anisotropy energy to the same order of magnitude as the spin-orbit coupling (see below).

An alternative to the CDFT approach is the heuristic suggestion by Brooks and coworkers [113–115] to use a $\boldsymbol{k}$-space method and to add a so-called orbital polarization (OP) term to the Hamilton matrix. This additional term has been borrowed from atomic theory and is meant to account for Hund's second rule, i.e. to maximize the orbital angular momentum. During the last years, this approach has been applied with remarkable success to d- as well as f-electron systems and has been refined by various authors [116,117]. As it could be shown [118], Brooks' OP-term can be formulated in a way that can be incorporated into the Dirac equation allowing that way for a corresponding extension of band structure methods based on multiple scattering theory [118]. For a d-electron system, i.e. for the case that orbital magnetism is primarily due to an open d-electron shell, Brooks' OP-term takes the form $-B_{m_s}\langle\hat{l}_\mathrm{z}\rangle_{m_s} m_l\,\delta_{l2}$. This term describes a shift in energy for an orbital with quantum numbers $l = 2$, m_l and m_s that is proportional to the average orbital angular momentum $\langle l_\mathrm{z}\rangle_{m_s}$ for the m_s-spin subsystem and the so-called Racah parameters B_{m_s} [119] that in turn can be represented by the Coulomb integrals $F^2_{m_s}$ and $F^4_{m_s}$. An operator that corresponds to this energy shift is given by

$$\mathcal{H}^{\mathrm{OP}}_{m_s} = -B^{\mathrm{OP}}_{m_s}(r)\langle\hat{l}_\mathrm{z}\rangle_{m_s}\hat{l}_\mathrm{z}\,\delta_{l2} \ , \tag{17}$$

with

$$B^{\mathrm{OP}}_{m_s}(r) = \frac{2}{441}\int[9\frac{r^2_<}{r^3_>} - 5\frac{r^4_<}{r^5_>}]\,\rho_{\mathrm{d}m_s}(r')4\pi r'^2\,dr' \ , \tag{18}$$

where $\rho_{\mathrm{d}m_s}$ describes the average charge density of a d-electron with spin character m_s. Obviously the operator $\mathcal{H}^{\mathrm{OP}}_{m_s}$ has the form expected within CDFT for rotational symmetry [105]. This is emphasized by introducing the vector potential function $A^{\mathrm{OP}}_{m_s} = -B^{\mathrm{OP}}_{m_s}(r)\langle l_{\mathrm{z}}\rangle$ that leads to the Dirac equation:

$$\left[\frac{\hbar}{\mathrm{i}}c\boldsymbol{\alpha}\cdot\boldsymbol{\nabla} + \beta mc^2 + V_{\mathrm{eff}}(\boldsymbol{r}) + \beta\boldsymbol{\sigma}\cdot\boldsymbol{B}_{\mathrm{eff}}(\boldsymbol{r}) + A^{\mathrm{OP}}\beta l_{\mathrm{z}}\right]\Psi_i(\boldsymbol{r}) = \epsilon_i\Psi_i(\boldsymbol{r})\,. \quad (19)$$

For a further discussion of the connection of this equation with CDFT see below.

In addition to the OP-formalism several alternative schemes have been suggested in the past to account within a relativistic band structure calculation for correlation effects not incorporated within the local approximation to SDFT (LSDA). For example the LDA+U-scheme has been applied to the compound CeSb [56], a system that has a maximum Kerr-rotation angle of 90° [120]. Similar experience has been made for other f-electron systems. Nevertheless, one should point out that by applying the LDA+U-scheme one leaves the framework of DFT. This does not apply to the SIC (self-interaction correction) formalism [96], for which a proper relativistic formulation has been worked out recently [121,122] and applied to magnetic solids [121].

From the above presentation it is obvious that relativistic effects influence the electronic structure in a twofold way. On the one hand side, one has the influence on the electronic kinetics, that is accounted for by working with the Dirac-formalism. On the other hand, relativity influences the electron-electron interaction via the retardation effect, the Breit-interaction and so on, leading to quite pronounced corrections for the exchange and correlation energy E_{xc} compared to its non-relativistic counterpart. This has been studied in detail for the paramagnetic and the spin-polarized case for example by MacDonald and Vosko [63,98], Rajagopal and coworkers [100,102,103] and Engel and coworkers [123]. Until now, however, only very few investigations have been done on the importance of these corrections [19,124–126]. Nevertheless, one may conclude from these few studies that the absolute magnitude of total energies as well as the binding energies of tightly bound core states is affected in a rather appreciable way. However, for properties like the equilibrium lattice parameter or even for magnetic properties no pronounced changes have to be expected. For this reason, the use of parameterizations derived within non-relativistic SDFT seems to be well justified.

2.2 Multiple scattering formalism

Solution of the Single Site Dirac Equation The first step to solve one of the above Dirac-equations for a solid using multiple scattering formalism is to find the solutions to the corresponding Dirac-equation for an isolated potential well. For that purpose Strange et al. [68] investigated the associated Lippmann-Schwinger-equation and derived a set of radial differential equations for the single-site solutions. An alternative scheme has been used by other authors [66,67] dealing with the problem by writing as a first step the single-site Dirac equation in spherical coordinates [7]. For the spin-polarized (SDFT)

case this leads to (for simplicity it is assumed in the following that one has $\boldsymbol{B}(\boldsymbol{r}) = B(r)\hat{\boldsymbol{e}}_{\rm z}$ and atomic Rydberg units will be used throughout):

$$\left[{\rm i}\gamma_5\sigma_r c \left(\frac{\partial}{\partial r} + \frac{1}{r} - \frac{\beta}{r}\hat{K} \right) + V + \beta\sigma_{\rm z} B + (\beta - 1)\,\frac{c^2}{2} - E \right] \psi_\nu = 0\ . \tag{20}$$

Here the spin-orbit operator $\hat{K}$ is defined by

$$\hat{K} = \beta(\boldsymbol{\sigma}\cdot\boldsymbol{l} + 1) \tag{21}$$

and the matrices γ_5 and σ_r are given by:

$$\gamma_5 = \begin{pmatrix} 0 & -I_2 \\ -I_2 & 0 \end{pmatrix} \tag{22}$$

and

$$\sigma_r = \hat{\boldsymbol{r}}\cdot\boldsymbol{\sigma}\ , \tag{23}$$

with $\boldsymbol{\sigma}$ the vector of the 4×4 Pauli matrices [7]. To find solutions to Eq. (20) one makes the ansatz:

$$\psi_\nu = \sum_{\Lambda} \psi_{\Lambda\nu}\ , \tag{24}$$

where the partial waves $\psi_{\Lambda\nu}$ are chosen to have the same form as the linearly independent solutions for a spherical symmetric potential:

$$\psi_\Lambda(\boldsymbol{r}, E) = \begin{pmatrix} g_\kappa(r, E)\,\chi_\Lambda(\hat{\boldsymbol{r}}) \\ i f_\kappa(r, E)\,\chi_{-\Lambda}(\hat{\boldsymbol{r}}) \end{pmatrix}\ . \tag{25}$$

Here the large and small components are composed of the radial wave functions $g_\kappa(r, E)$ and $f_\kappa(r, E)$ and the spin-angular functions:

$$\chi_\Lambda(\hat{\boldsymbol{r}}) = \sum_{m_s = \pm 1/2} C(l\tfrac{1}{2}j; \mu - m_s, m_s)\, Y_l^{\mu - m_s}(\hat{\boldsymbol{r}})\,\chi_{m_s}\ , \tag{26}$$

with the Clebsch-Gordon coefficients $C(l\frac{1}{2}j; m_l, m_s)$, the complex spherical harmonics $Y_l^{m_l}$ and the Pauli-spinors χ_{m_s}. The spin-orbit and magnetic quantum numbers κ and μ, respectively, have been combined to $\Lambda = (\kappa, \mu)$ and $-\Lambda = (-\kappa, \mu)$, respectively. The spin-angular functions $\chi_\Lambda(\hat{\boldsymbol{r}})$ are simultaneous eigenfunctions of the operators $\boldsymbol{j}^2$, $j_{\rm z}$ and $\hat{K}$ with $\boldsymbol{j} = \boldsymbol{l} + \frac{1}{2}\boldsymbol{\sigma}$. The corresponding eigenvalues are $j(j+1)$, μ and $-\kappa$ and are connected by the following relations:

$$\kappa = \begin{cases} -l - 1 \text{ for } j = l + 1/2 \\ +l \quad \text{for } j = l - 1/2 \end{cases} \tag{27}$$

$$j = |\kappa| - 1/2 \tag{28}$$

$$-j \le \mu \le +j \tag{29}$$

$$\bar{l} = l - S_\kappa\ , \tag{30}$$

where $S_\kappa = \kappa/|\kappa|$ is the sign of κ and $\bar{l}$ is the orbital angular momentum quantum number belonging to $\chi_{-\Lambda}$.

Inserting the ansatz in Eq. (24) into the single-site Dirac-equation (20) and integrating over the angles leads to the following set of radial differential equations:

$$P'_{\Lambda\nu} = -\frac{\kappa}{r} P_{\Lambda\nu} + \left[\frac{E-V}{c^2} + 1\right] Q_{\Lambda\nu} + \frac{B}{c^2} \sum_{\Lambda'} \langle \chi_{-\Lambda} | \sigma_z | \chi_{-\Lambda'} \rangle Q_{\Lambda'\nu} \tag{31}$$

$$Q'_{\Lambda\nu} = \frac{\kappa}{r} Q_{\Lambda\nu} - [E-V]\, P_{\Lambda\nu} + B \sum_{\Lambda'} \langle \chi_\Lambda | \sigma_z | \chi_{\Lambda'} \rangle P_{\Lambda'\nu}\,, \tag{32}$$

where the usual notation $P_{\Lambda\nu} = r g_{\Lambda\nu}$ and $Q_{\Lambda\nu} = c r f_{\Lambda\nu}$ has been used. The coupling coefficients occurring here are given by:

$$\langle \chi_\Lambda | \sigma_z | \chi_{\Lambda'} \rangle = G(\kappa, \kappa', \mu)\, \delta_{\mu\mu'} \tag{33}$$

$$= \delta_{\mu\mu'} \begin{cases} -\frac{\mu}{(\kappa+1/2)} & \text{for} \quad \kappa = \kappa' \\ -\sqrt{1 - (\frac{\mu}{\kappa+1/2})^2} & \text{for} \quad \kappa = -\kappa' - 1 \\ 0 & \text{otherwise} \end{cases} . \tag{34}$$

Because of the properties of $G(\kappa, \kappa', \mu)$ only partial waves for the same μ get coupled; i.e. μ is still a good quantum number. In addition, one can see that for the orbital angular momentum quantum numbers l and l' of two coupled partial waves one has the restriction $l - l' = 0, \pm 2, \ldots$, i.e. only waves of the same parity are coupled. Nevertheless, this still implies that an infinite number of partial waves are coupled. In practice, however, all coupling terms for which $l - l' = \pm 2$ are ignored. A justification for this restriction has been given by Feder et al. [67] and Cortona et al. [127]. Results of numerical studies furthermore justify this simplification [128,129]. Altogether, this restricts the number of terms in Eqs. (31) and (32) to 2 if $|\mu| < j$. For the case $\mu = j$, there is no coupling at all; i.e. the solutions ψ_ν have pure spin-angular character Λ.

The procedure sketched above to derive, starting from the SDFT-Dirac equation, the corresponding set of coupled radial differential equations can be used straightforwardly for more complex situations. In the case of the formally rather simple Brooks' OP-formalism one has the additional term $\mathcal{H}^{\mathrm{OP}}_{m_s}$ (see Eq. (17)) leading to the radial equations:

$$P'_{\Lambda\nu} = -\frac{\kappa}{r} P_{\Lambda\nu} + \left[\frac{E-V}{c^2} + 1\right] Q_{\Lambda\nu} + \frac{B}{c^2} \sum_{\Lambda'} \langle \chi_{-\Lambda} | \sigma_z | \chi_{-\Lambda'} \rangle Q_{\Lambda'\nu} - \frac{1}{c^2} \sum_{\Lambda'} \langle \chi_{-\Lambda} | A^{\mathrm{OP}} l_z | \chi_{-\Lambda'} \rangle Q_{\Lambda'} \tag{35}$$

$$Q'_{\Lambda\nu} = \frac{\kappa}{r} Q_{\Lambda\nu} - [E-V]\, P_{\Lambda\nu} + B \sum_{\Lambda'} \langle \chi_\Lambda | \sigma_z | \chi_{\Lambda'} \rangle P_{\Lambda'\nu} - \sum_{\Lambda'} \langle \chi_\Lambda | A^{\mathrm{OP}} l_z | \chi_{\Lambda'} \rangle P_{\Lambda'}\,. \tag{36}$$

Formally, the term $\mathcal{H}_{m_s}^{\mathrm{OP}}$ can be seen to represent the coupling of the electronic orbital current to a vector potential $\boldsymbol{A}$. A more general form of such a vector potential is encountered for example when one is including the Breit interaction in the Dirac equation. To deal with such a situation, it is most convenient to represent the vectors within the scalar product $\boldsymbol{\alpha}\cdot\boldsymbol{A}$ (see Eq. (1)) using spherical coordinates and to expand the spatial dependency of the components of the vector potential $\boldsymbol{A}$ in terms of complex spherical harmonics:

$$\boldsymbol{\alpha}\cdot\boldsymbol{A} = \sum_{m} \alpha_m i \sum_{LM} A_{LM}^{m}(r) Y_{L}^{-m}(\hat{\boldsymbol{r}}) \; . \tag{37}$$

When added to the SDFT-Dirac-Hamiltonian this leads to the following radial equations [112]:

$$\begin{aligned} P'_{\Lambda\nu} \; = & -\frac{\kappa}{r} P_{\Lambda\nu} + \left[\frac{E-V}{c^2} + 1\right] Q_{\Lambda\nu} + \frac{B}{c^2} \sum_{\Lambda'} \langle \chi_{-\Lambda} | \sigma_{\mathrm{z}} | \chi_{-\Lambda'} \rangle Q_{\Lambda'\nu} \\ & - \frac{1}{c} \sum_{\Lambda'} \sum_{LMm} A_{LM}^{m} \langle \chi_{-\Lambda} | Y_{L}^{M} \sigma_m | \chi_{\Lambda'} \rangle P_{\Lambda'} \end{aligned} \tag{38}$$

$$\begin{aligned} Q'_{\Lambda\nu} = & \frac{\kappa}{r} Q_{\Lambda\nu} - [E-V]\, P_{\Lambda\nu} + B \sum_{\Lambda'} \langle \chi_{\Lambda} | \sigma_{\mathrm{z}} | \chi_{\Lambda'} \rangle P_{\Lambda'\nu} \\ & - \frac{1}{c} \sum_{\Lambda'} \sum_{LMm} A_{LM}^{m} \langle \chi_{\Lambda} | Y_{L}^{M} \sigma_m | \chi_{-\Lambda'} \rangle Q_{\Lambda'} \; . \end{aligned} \tag{39}$$

The Dirac equation Eq. (14) set up within the framework of CDFT can be treated in a completely analogous way resulting in a similar set of radial differential equations for large and small component wave functions.

Because of the high symmetry of the orbital polarization Hamiltonian $\mathcal{H}_{m_s}^{\mathrm{OP}}$ no coupling between partial waves beyond that caused by the spin-dependent part of the SDFT-Dirac-Hamiltonian is introduced. This holds also if a vector potential term is added to the Hamiltonian that stems from the Breit-interaction or from the CDFT-formalism, as long as one imposes for this rotational symmetry, with the symmetry axes coinciding with the direction of the magnetization.

The problem of deriving a full-potential (FP) version of the KKR-formalism has been discussed in a rather controversial way during the last decades. Now, it is generally accepted that the scheme proposed among others by Dederichs, Zeller and coworkers [130,131] supplies a sound basis for FP-KKR band structure calculations. This implies that in a first step space is subdivided into non-overlapping, space-filling polyhedra usually obtained by means of the Wigner-Seitz-construction. The shape of these Wigner-Seitz cells is represented by the so called shape functions $\Theta_L(r)$ [132] with

$$\Theta_{\mathrm{WS}}(\boldsymbol{r}) = \sum_{L} \theta_L(r) \mathcal{Y}_L(\hat{\boldsymbol{r}}) \; , \tag{40}$$

where the step function $\Theta_{\rm WS}$ is 1 for $\boldsymbol{r}$ within the cell and 0 otherwise. The functions $\mathcal{Y}_L$ are real spherical harmonics with L standing for (l,m). In addition one defines the radius $r_{\rm cr}$ of the smallest circumscribed sphere, for which $\Theta_{\rm WS}(\boldsymbol{r}) = 0$ for $r > r_{\rm cr}$. Multiplying the potential V of the extended system in Eq. (9) with the function $\Theta_{\rm WS}(\boldsymbol{r})$ centered at an atomic site n leads to the single site problem. To solve the corresponding single site Dirac equation the same ansatz as given in Eqs. (24) and (25) is made. This leads now to the coupled radial Dirac equations:

$$P'_{\Lambda} = -\frac{\kappa}{r} P_{\Lambda} + \left[\frac{E}{c^2} + 1\right] Q_{\Lambda} - \frac{1}{c^2} \sum_{\Lambda'} V^{-}_{\Lambda\Lambda'} Q_{\Lambda'} \tag{41}$$

$$Q'_{\Lambda} = \frac{\kappa}{r} Q_{\Lambda} - E P_{\Lambda} + \sum_{\Lambda'} V^{+}_{\Lambda\Lambda'} P_{\Lambda'} \ . \tag{42}$$

Here the underlying Dirac-Hamiltonian has been restricted to the SDFT-form with the corresponding potential matrix elements $V^{\pm}_{\Lambda\Lambda'}$ defined by

$$V^{\pm}_{\Lambda\Lambda'}(r) = \langle \chi_{\pm\Lambda} | V_{\rm eff} \pm \boldsymbol{\sigma}\boldsymbol{B} | \chi_{\pm\Lambda'} \rangle \ . \tag{43}$$

These are straightforwardly evaluated by expanding the potential into real spherical harmonics:

$$V(\boldsymbol{r}) \qquad = \sum_{L} V_L(r) \mathcal{Y}_L(\hat{\boldsymbol{r}}) \tag{44}$$

$$B(\boldsymbol{r}) \qquad = \sum_{L} B_L(r) \mathcal{Y}_L(\hat{\boldsymbol{r}}) \tag{45}$$

$$\text{with } \boldsymbol{B}(\boldsymbol{r}) = B(\boldsymbol{r}) \hat{\boldsymbol{B}} \ .$$

Here it has been assumed that $\boldsymbol{B}(\boldsymbol{r})$ points everywhere along the same direction $\hat{\boldsymbol{B}}$. In the following applications $\hat{\boldsymbol{B}}$ will be oriented along the z-axis. However, these are no necessary restrictions for the formalism; i.e. treatment of other orientations or non-collinear magnetic states can be straightforwardly accounted for.

Compared to a muffin-tin or atomic sphere approximation potential construction inclusion of non-spherical terms in V and B obviously leads to further coupling. In practice, however, the number of coupled partial waves is restricted to $2(l_{\max}+1)^2$ by fixing an upper limit $l_{\max}$ for the angular momentum expansion of the wave function in Eq. (24). For example, for $l_{\max} = 2$ one may have up to 18 partial waves coupled; i.e., one has to solve up to 36 coupled equations for the functions P_{Λ} and Q_{Λ}. However, for a cubic system with $\hat{\boldsymbol{B}} = \hat{\boldsymbol{z}}$ and $l_{\max} = 2$ one has at most 3 partial waves coupled due to the high symmetry of the system.

Single-site t-matrix and Normalization of the Wave Functions Working with one of the above versions of the Dirac equation and using the corresponding coupled radial differential equations a set of $2(l_{\max}+1)^2$ linearly independent regular solutions Φ_{Λ} can be created by initializing the outward integration with

a selected spin-angular character Λ dominating close to the nucleus; i.e. one demands that:

$$\Phi_{\Lambda}(\boldsymbol{r}, E) = \sum_{\Lambda'} \Phi_{\Lambda'\Lambda}(\boldsymbol{r}, E) \stackrel{r \to 0}{\longrightarrow} \Phi_{\Lambda\Lambda}(\boldsymbol{r}, E) \; . \tag{46}$$

After having solved all systems of coupled equations for the wave functions Φ_{Λ} one gets the corresponding single site t-matrix by introducing the auxiliary matrices a and b [133–135]:

$$a_{\Lambda\Lambda'}(E) = -\mathrm{i}pr^2[h^-_{\Lambda}(p\boldsymbol{r}), \Phi_{\Lambda\Lambda'}(\boldsymbol{r}, E)]_r \tag{47}$$

$$b_{\Lambda\Lambda'}(E) = \mathrm{i}pr^2[h^+_{\Lambda}(p\boldsymbol{r}), \Phi_{\Lambda\Lambda'}(\boldsymbol{r}, E)]_r \; . \tag{48}$$

Here $p = \sqrt{E(1 + E/c^2)}$ is the relativistic momentum [7] and $[\ldots]_r$ denotes the relativistic form of the Wronskian [135]:

$$[h^+_{\Lambda}, \phi_{\Lambda\Lambda'}]_r = h^+_l c f_{\Lambda\Lambda'} - \frac{p}{1 + E/c^2} S_{\kappa} h^+_{\bar{l}} g_{\Lambda\Lambda'} \; . \tag{49}$$

The functions $h^{\pm}_{\Lambda}$ are the relativistic version of the Hankel functions of the first and second kind [7]:

$$h^{\pm}_{\Lambda}(p\boldsymbol{r}) = \sqrt{\frac{1 + E/c^2}{c^2}} \begin{pmatrix} h^{\pm}_l(pr)\chi_{\Lambda}(\hat{\boldsymbol{r}}) \\ \frac{ipcS_{\kappa}}{E+c^2} h^{\pm}_{\bar{l}}(pr)\chi_{\bar{\Lambda}}(\hat{\boldsymbol{r}}) \end{pmatrix} \; . \tag{50}$$

Evaluating all functions in Eqs. (47) – (48) at $r_{\mathrm{b}} = r_{\mathrm{mt}}$, r_{WS} or r_{cr}, resp., i.e. the muffin-tin, the Wigner-Seitz or the critical radius depending on whether one is using the muffin-tin, the ASA- or full-potential mode, one finally has [135]:

$$t(E) = \frac{i}{2p}(a(E) - b(E))b^{-1}(E) \; . \tag{51}$$

By a superposition of the wave functions Φ_{Λ} according to the boundary conditions

$$\begin{aligned} Z_{\Lambda}(\boldsymbol{r}, E) &= \sum_{\Lambda'} Z_{\Lambda'\Lambda}(\boldsymbol{r}, E) \\ &\stackrel{r > r_{\mathrm{b}}}{\longrightarrow} \sum_{\Lambda'} j_{\Lambda'}(\boldsymbol{r}, E) t(E)^{-1}_{\Lambda'\Lambda} - iph^+_{\Lambda}(\boldsymbol{r}, E) \end{aligned} \tag{52}$$

one gets an alternative set of linearly independent regular solutions Z_{Λ} to the single site Dirac equation. These functions are normalized in analogy to non-relativistic multiple scattering theory according to the convention of Faulkner and Stocks [10] and allow straightforwardly to set up the electronic Green's function (see below). The additionally needed irregular solutions J_{Λ} are fixed by the boundary condition

$$J_{\Lambda}(\boldsymbol{r}, E) \stackrel{r \to r_{\mathrm{b}}}{\longrightarrow} j_{\Lambda}(\boldsymbol{r}, E) \tag{53}$$

and are obtained just by inward integration. The functions j_{Λ} occurring in Eqs. (52) – (53) are the relativistic counterpart to the spherical Bessel functions defined in analogy to Eq. (50) for $h^{\pm}_{\Lambda}$ [7].

Manipulation of the SDFT-Dirac-Hamiltonian Dealing with relativistic effects by adding corresponding corrections to the Schrödinger equation allows one straightforwardly to investigate the role of these corrections individually. For the fully relativistic Dirac formalism sketched above this is obviously not the case. The only way to monitor the importance of all relativistic effects in a consistent way is to manipulate them simultaneously by scaling the speed of light c. To allow in spite of this for a separate investigation of the role of scalar-relativistic effects and the spin-orbit coupling an elimination scheme has been applied recently to the SDFT-Dirac Hamiltonian.

Using this procedure an equation for the large component wave function $\phi(\boldsymbol{r}, E)$ can be introduced that is still exact [137,138]:

$$\left[-\frac{1}{r^2}\frac{\partial}{\partial r}r^2\frac{\partial}{\partial r}+\frac{\hat{l}^2}{r^2}-S_{\Lambda}T+S_{\Lambda}B\sigma_{\mathrm{z}}\right.$$
$$\left.+\frac{S'_{\Lambda}}{S_{\Lambda}}\left(\frac{\mathrm{d}}{\mathrm{d}r}-\frac{1}{r}-\frac{\hat{K}-1}{r}\right)\right]\phi(\boldsymbol{r},E) \quad =0\,. \tag{54}$$

Here the abbreviations

$$T \;=E-V \tag{55}$$
$$S_{\Lambda}=\frac{E-V}{c^2}+1+\frac{B}{c^2}\langle\chi_{-\Lambda}|\sigma_{\mathrm{z}}|\chi_{-\Lambda}\rangle \tag{56}$$

have been used, where S_{Λ} would be identical to 1 in the non-relativistic limit which is obtained for $c\to\infty$.

For the wave function $\phi(\boldsymbol{r}, E)$ the ansatz

$$\phi(\boldsymbol{r},E)=\sum_{\Lambda}\phi_{\Lambda}(\boldsymbol{r},E)=\sum_{\Lambda}g_{\Lambda}(r,E)\chi_{\Lambda}(\hat{\boldsymbol{r}})\,, \tag{57}$$

is made in accordance with the adopted Λ-representation. Inserting this ansatz into the wave equation (54) leads to the following second order radial differential equation:

$$P''_{\Lambda}=\frac{l\,(l+1)}{r^2}\,P_{\Lambda}-S_{\Lambda}\,TP_{\Lambda}+S_{\Lambda}\sum_{\Lambda'}B_{\Lambda\Lambda'}\,P_{\Lambda'}$$
$$+\frac{S'_{\Lambda}}{S_{\Lambda}}\left[\frac{\mathrm{d}}{\mathrm{d}r}-\frac{1}{r}\right]P_{\Lambda}+\frac{S'_{\Lambda}}{S_{\Lambda}}\frac{1}{r}\sum_{\Lambda'}\xi_{\Lambda\Lambda'}\,P_{\Lambda'} \tag{58}$$

with the spin-orbit coupling operator $\hat{K}$ replaced using the operator

$$\hat{\xi}=\hat{K}-1=\boldsymbol{\sigma}\cdot\boldsymbol{l}\,. \tag{59}$$

Inserting the proper values for the corresponding angular matrix elements

$$\xi_{\Lambda\Lambda'}=\langle\chi_{\Lambda}|\hat{K}-1|\chi_{\Lambda'}\rangle=(-\kappa-1)\delta_{\Lambda\Lambda'}\,, \tag{60}$$

the exact second order differential equation for the major component is recovered.

Replacing the spin-orbit coupling operator $\hat{K}$ in Eqs. (59) and (60) by its scaled counterpart

$$\hat{K}_x = 1 + x\,\boldsymbol{\sigma}\cdot\boldsymbol{l} \tag{61}$$

with the associated effective spin-orbit quantum number

$$\kappa_x = -1 + x\,(1+\kappa)\,, \tag{62}$$

allows one to scale the strength of the spin-orbit coupling separately. Obviously, setting $x = 1$ nothing changes at all, while for $x = 0$ one gets $\kappa_x = -1$. This is just the value of the spin-orbit quantum number for s-states where there is no spin-orbit coupling. Therefore, replacing κ in Eq. (60) by κ_x switches the spin-orbit coupling off for any partial wave if $x = 0$ and reduces or increases the spin-orbit coupling strength else.

To solve the resulting second order differential equation Eq. (58) for the wave functions $P_\Lambda(r, E)$ the auxiliary function $Q_\Lambda(r, E)$ is introduced by the definition

$$Q_\Lambda = \left[P'_\Lambda + \frac{\kappa_x}{r}\,P_\Lambda\right]\frac{1}{S_\Lambda}\,. \tag{63}$$

This leads after some simple transformations to a coupled set of first order differential equations:

$$P'_\Lambda = -\frac{\kappa_x}{r}\,P_\Lambda + S_\Lambda Q_\Lambda \tag{64}$$

$$Q'_\Lambda = \frac{\kappa_x}{r}\,Q_\Lambda - TP_\Lambda + \sum_{\Lambda'} B_{\Lambda\Lambda'}\,P_{\Lambda'} + \frac{l\,(l+1) - \kappa_x(\kappa_x+1)}{r^2}\,\frac{1}{S_\Lambda}P_\Lambda\,. \tag{65}$$

Apart from allowing one to manipulate the strength of the spin-orbit coupling, Eq. (58) also permits to modify the form of the spin-orbit coupling operator. For this purpose $\hat{\xi}$ is splited according to

$$\begin{aligned}\hat{\xi} &= \boldsymbol{\sigma}\cdot\boldsymbol{l}\\ &= \sigma_{\mathrm{z}} l_{\mathrm{z}} + (\sigma_{\mathrm{x}} l_{\mathrm{x}} + \sigma_{\mathrm{y}} l_{\mathrm{y}})\\ &= \hat{\xi}_{\mathrm{zz}} + \hat{\xi}_{\mathrm{xy}}\end{aligned} \tag{66}$$

into two parts. The first term, $\hat{\xi}_{\mathrm{zz}}$, gives rise only to a splitting of levels with different quantum numbers m_l. Because no mixing of states with different spin character is introduced that way, m_s is left as a good quantum number. In contrast to this, the second term, $\hat{\xi}_{\mathrm{xy}}$, gives rise to a hybridization of different spin states while no obvious splitting of m_l-levels is caused by it. Because the two parts of $\hat{\xi}$ have quite different consequences it is interesting to investigate

their effect separately by replacing $\hat{\xi}$ in Eq. (58) either by $\hat{\xi}_{\rm zz}$ or by $\hat{\xi}_{\rm xy}$. The corresponding angular matrix elements to be inserted are

$$\langle\chi_\Lambda|\hat{\xi}_{\rm zz}|\chi_{\Lambda'}\rangle = \delta_{ll'}\delta_{\mu\mu'}\begin{cases} -\mu\sqrt{1-\left(\frac{2\mu}{2l+1}\right)^2} & \text{for } \kappa \neq \kappa' \\ -S_\kappa \frac{2\mu^2}{2l+1} - \frac{1}{2} & \text{for } \kappa = \kappa' \end{cases} \tag{67}$$

$$\langle\chi_\Lambda|\hat{\xi}_{\rm xy}|\chi_{\Lambda'}\rangle = \delta_{ll'}\delta_{\mu\mu'}\begin{cases} +\mu\sqrt{1-\left(\frac{2\mu}{2l+1}\right)^2} & \text{for } \kappa \neq \kappa' \\ -\kappa + S_\kappa \frac{2\mu^2}{2l+1} - \frac{1}{2} & \text{for } \kappa = \kappa' \,. \end{cases} \tag{68}$$

A solution of the resulting second order differential equation for the two different cases can again be achieved by introducing the auxiliary function Q_Λ in Eq. (63). This leads to the following sets of coupled first order differential equations:

$$P'_\Lambda = -\frac{\kappa}{r} P_\Lambda + S_\Lambda Q_\Lambda \tag{69}$$

$$\begin{aligned} Q'_\Lambda = {} & \frac{\kappa}{r} Q_\Lambda - T P_\Lambda + \sum_{\Lambda'} B_{\Lambda\Lambda'} P_{\Lambda'} \\ & - \frac{S'_\Lambda}{S_\Lambda}\frac{1}{r}\left[(\kappa+1)P_\Lambda + \sum_{\Lambda'} \xi^\lambda_{\Lambda\Lambda'} P_{\Lambda'}\right], \end{aligned} \tag{70}$$

with $\xi^\lambda_{\Lambda\Lambda'} = \langle\chi_\Lambda|\hat{\xi}_{\rm zz}|\chi_{\Lambda'}\rangle$ or $\xi^\lambda_{\Lambda\Lambda'} = \langle\chi_\Lambda|\hat{\xi}_{\rm xy}|\chi_{\Lambda'}\rangle$, respectively.

The final coupled radial equations obtained for the two manipulation schemes sketched above differ only with respect to the last term in Eqs. (65) and (70), respectively, from the original equation (31) for their small component wave function corresponding to the proper SDFT-Dirac-Hamiltonian. Implementation of the two manipulation schemes therefore requires only minor modifications in the corresponding programs.

However, one has to keep in mind that $Q_\Lambda(r, E)$ defined by Eq. (63) has not the meaning of a small component occurring within the bi-spinor formalism. For this reason the boundary conditions to match the wave functions to solutions outside the sphere boundary have to be specified by $P_\Lambda(r, E)$ alone [57]. To set up the corresponding single site t-matrix $t_{\Lambda\Lambda'}(E)$ used within the KKR-formalism one therefore has to replace the relativistic Wronskian (see Ref. [135]) by its standard form $g_\Lambda(r, E)j'_l(r, E) - g'_\Lambda(r, E)j_l(r, E)$ with $j_l(r, E)$ the spherical Bessel function. Furthermore, one has to note that for the evaluation of the matrix elements of any operator it has to be transformed in such a way that no coupling of large and small component occurs. This applies, for example, to the operator $\boldsymbol{\alpha}\cdot\boldsymbol{A}$ that describe the interaction of electrons with the vector potential $\boldsymbol{A}$. In this case, for example, the $\boldsymbol{\nabla}\cdot\boldsymbol{A}$-form of the matrix elements can be used [42,139].

Green's function The problem of setting up the electronic Green's function $G(\boldsymbol{r}, \boldsymbol{r}'E)$ for a solid on the basis of relativistic multiple scattering theory for

arbitrary scalar and vector potentials has been investigated in great detail by Tamura [79]. In analogy to the non-relativistic formalism of Faulkner and Stocks [10] the Green's function $G(\boldsymbol{r}, \boldsymbol{r}\,', E)$ can be written as:

$$\begin{aligned} G(\boldsymbol{r}, \boldsymbol{r}\,', E) = & \sum_{\Lambda\Lambda'} Z^n_\Lambda(\boldsymbol{r}, E)\tau^{nn'}_{\Lambda\Lambda'}(E) Z^{n'\times}_{\Lambda'}(\boldsymbol{r}\,', E) \\ & - \sum_{\Lambda} \big[\, Z^n_\Lambda(\boldsymbol{r}, E) J^{n\times}_\Lambda(\boldsymbol{r}\,', E)\Theta(r' - r) \\ & + J^n_\Lambda(\boldsymbol{r}, E) Z^{n\times}_\Lambda(\boldsymbol{r}\,', E)\Theta(r - r') \,\big]\, \delta_{nn'} \end{aligned} \tag{71}$$

for $\boldsymbol{r}$ ($\boldsymbol{r}\,'$) within the cell n (n'). Here the quantity $\tau^{nn'}_{\Lambda\Lambda'}(E)$ is the so-called scattering path operator [140] that represents all multiple scattering events in a many-atom system in a consistent way (see below). The wave functions Z^n_Λ and J^n_Λ are the properly normalized regular and irregular solutions of the corresponding single site problem for site n (see above).

The most important technical point to note is that in Eq. (71) the sign "$\times$" indicates that the wave functions $Z^\times$ and $J^\times$ are the left-hand side regular and irregular solutions of the corresponding modified Dirac equation [79]. Fortunately, for the SDFT-Dirac-Hamiltonian these are obtained from the same radial differential equations as the conventional right-hand side solutions Z_Λ and J_Λ; i.e. from Eqs. (41)-(42) with the potential matrix elements $V^{\pm}_{\Lambda\Lambda'}$ replaced by $V^{\pm}_{\Lambda'\Lambda}$. For highly symmetric systems one may have the situation that $V^{\pm}_{\Lambda\Lambda'} = V^{\pm}_{\Lambda'\Lambda}$. In this case $Z^\times$ and $J^\times$ are obtained from Z and J by simple complex conjugation and transposition:

$$Z^\times_\Lambda(\boldsymbol{r}, E) = \sum_{\Lambda'} (g_{\Lambda'\Lambda}(r, E)\chi^\dagger_{\Lambda'}(\hat{\boldsymbol{r}}); -i f_{\Lambda'\Lambda}(r, E)\chi^\dagger_{\bar{\Lambda}'}) \tag{72}$$

and

$$J^\times_\Lambda(\boldsymbol{r}, E) = \sum_{\Lambda'} (\tilde{g}_{\Lambda'\Lambda}(r, E)\chi^\dagger_{\Lambda'}(\hat{\boldsymbol{r}}); -i \tilde{f}_{\Lambda'\Lambda}(r, E)\chi^\dagger_{\bar{\Lambda}'}) \,, \tag{73}$$

since left and right hand side solutions are identical with respect to their radial parts. This applies in particular to the single site problem with spherically symmetric potential terms V and B, but also to cubic systems with the magnetization along the z-axis, as investigated here. Fortunately, this is still true if the OP-term is included in the Dirac equation (19) because here the relation (Eq. (11) in [79]) for the vector potential corresponding to the OP-potential term in Eq. (19) holds.

Calculation of the Scattering Path Operator $\boldsymbol{\tau^{nn'}_{\Lambda\Lambda'}}$ The scattering path operator $\tau^{nn'}_{\Lambda\Lambda'}$ – introduced by Gyorffy and Stott [140] – transfers a wave with spin-angular character Λ' coming in at site n' into a wave outgoing from site n with character Λ and with all possible scattering events that may take place in

between accounted for. According to this definition it has to fulfill the following self-consistency condition:

$$\underline{\tau}^{nn'} = \underline{t}^n \delta_{nn'} + \underline{t}^n \sum_{k \neq n} \underline{G}^{nk} \underline{\tau}^{kn'} \ , \tag{74}$$

where all quantities are energy dependent and the underline denotes matrices with their elements labeled by $\Lambda = (\kappa, \mu)$. Here the single site t-matrix $\underline{t}^n$ is fixed by the solutions to the single-site Dirac equation for site n. Furthermore, $\underline{G}^{nn'}$ is the relativistic real space Green's function or structure constants matrix that represents the propagation of a free electron between sites n and n' [133]. It is related to its non-relativistic counterparts $G^{nn'}_{\mathcal{L}\mathcal{L}'} = G^{nn'}_{LL'} \delta_{m_s m'_s}$ by the simple relation [80]:

$$G^{nn'}_{\Lambda\Lambda'} = (1 + E/c^2) \sum_{\mathcal{L}\mathcal{L}'} S^{+}_{\Lambda\mathcal{L}} G^{nn'}_{\mathcal{L}\mathcal{L}'} S_{\mathcal{L}'\Lambda'} \ , \tag{75}$$

where $\mathcal{L}$ and L stand as usual for the sets (l, m_l, m_s) and (l, m_l), resp., of non-relativistic quantum numbers. The matrix elements of the unitary transformation matrix $\underline{S}$ occurring in Eq. (75) are given by the Clebsch Gordon coefficients $C(l\frac{1}{2}j, \mu - m_s, m_s)$ [7].

For many situations it is often sufficient to consider a system consisting of only a finite number of atoms, as for example within the local interaction zone (LIZ) formalism [78] or EXAFS-theory [76,77]. In that case Eq. (74) can be solved by inverting the corresponding real-space KKR-matrix [77]:

$$\underline{\tau} = [\underline{\underline{m}} - \underline{\underline{G}}]^{-1} \ , \tag{76}$$

where the double underline indicates super-matrices with the elements being labeled by the site indices of the cluster. The elements themselves are matrices labeled by Λ as for example $(\underline{G})^{nn'} = \underline{G}^{nn'}$ with $(\underline{G}^{nn'})_{\Lambda\Lambda'} = G^{nn'}_{\Lambda\Lambda'}$. The matrix $\underline{\underline{m}}$ in Eq. (76) is site-diagonal and has the inverse of the single site t-matrix $\underline{t}^n$ as its diagonal elements; i.e. $(\underline{\underline{m}})^{nn'} = \underline{m}^n \delta_{nn'} = (\underline{t}^n)^{-1} \delta_{nn'}$.

Alternatively one may instert Eq. (74) repeatedly into itself to arrive at the scattering path expansion

$$\begin{aligned} \underline{\tau}^{nn} = \underline{t}^n &+ \underline{t}^n \sum_{k \neq n} \underline{G}^{nk} \underline{t}^k \underline{G}^{kn} \underline{t}^n \\ &+ \underline{t}^n \sum_{k \neq n} \sum_{l \neq k} \underline{G}^{nk} \underline{t}^k \underline{G}^{kl} \underline{t}^l \underline{G}^{ln} \underline{t}^n + ... \end{aligned} \tag{77}$$

for the site-diagonal scattering path operator $\underline{\tau}^{nn}$. Compared to the matrix inversion the scattering path expansion technique is highly efficient. On the other hand, one may encounter convergence problems using it. To avoid these problems several alternative and efficient schemes have been suggested in the literature [141,142] that have not been applied so far for relativistic calculations.

For ordered infinite systems Eq. (74) can be solved exactly by means of Fourier-transformation. For one atom per unit cell, the term $\tau_{\Lambda\Lambda'}^{nn'}$ is obtained from the Brillouin-zone integral

$$\tau_{\Lambda\Lambda'}^{nn'}(E) = \frac{1}{\Omega_{\rm BZ}} \int\limits_{\Omega_{\rm BZ}} d^3k [\underline{t}^{-1}(E) - \underline{G}(\boldsymbol{k}, E)]^{-1}_{\Lambda\Lambda'} e^{i\boldsymbol{k}(\boldsymbol{R}_n - \boldsymbol{R}_{n'})} \; . \tag{78}$$

Here $\boldsymbol{R}_{n(n')}$ denotes the lattice vector for site $n(n')$ and the relativistic $\boldsymbol{k}$-dependent structure constant matrix $\underline{G}(\boldsymbol{k}, E)$ is connected to its non-relativistic counterpart in analogy to Eq. (75) for the real space formulation.

As usual, group theory can be exploited to restrict the integration in Eq. (78) to the irreducible part of the Brillouin-zone, that depends on the orientation of the magnetization [143,144]. For cubic systems, the site-diagonal case $n = n'$ has been dealt with in detail by Hörmandinger and Weinberger [145], while the site-off-diagonal case $n \neq n'$ has been worked out by Zecha and Kornherr [146,147].

To deal with the electronic structure of surfaces within the framework of the spin-polarized relativistic KKR-formalism, the standard layer techniques used for LEED and photoemission investigations [148] have been generalized by several authors [90,149]. As an alternative to this, Szunyogh and coworkers introduced the TB-version of the KKR-method [74,150,75]. To invert the emerging layer-, $\boldsymbol{k}_{\parallel}$- and Λ-indexed KKR-matrix, that has in principle an infinite number of rows and columns, these authors applied techniques that are also used within the TB-LMTO-Green's function formalism [95]. Finally, the scheme to deal with surfaces and layered systems developed by Dederichs and coworkers [151], that represents the vacuum region by layers of empty atomic sites, has been generalized recently by Huhne and Nonas [152,153].

Treatment of Disordered Alloys One of the appealing features of the multiple scattering formalism described above is that it can be applied straightforwardly to deal with disordered alloys. Within the Coherent Potential Approximation (CPA) [154] alloy theory the configurationally averaged properties of a disordered alloy are represented by a hypothetical ordered CPA-medium, which in turn may be described by a corresponding scattering path operator $\tau_{\Lambda\Lambda'}^{nn,\rm CPA}$. This operator is determined by the CPA-condition:

$$x_{\rm A} \underline{\tau}^{nn,\rm A} + x_{\rm B} \underline{\tau}^{nn,\rm B} = \underline{\tau}^{nn,\rm CPA} \; , \tag{79}$$

where the matrices are defined with respect to the index Λ and the binary alloy system has components A and B at relative concentrations $x_{\rm A}$ and $x_{\rm B}$, respectively. The above equation represents the requirement that the concentration-weighted sum of the component-projected scattering path operators $\underline{\tau}^{nn,\alpha}$ should be identical to that of the CPA-medium; i.e. embedding an A- or a B-atom into the CPA-medium should not cause any additional scattering.

The $\underline{\tau}^{nn,\alpha}$ describes the scattering properties of an α-atom embedded in the CPA-medium, i.e. of a substitutional impurity and is given by the expression

$$\underline{\tau}^{nn,\alpha} = \underline{\tau}^{nn,\rm CPA} \left[1 + \left(\underline{t}_{\alpha}^{-1} - \underline{t}_{\rm CPA}^{-1} \right) \underline{\tau}^{nn,\rm CPA} \right]^{-1} \; , \tag{80}$$

where $\underline{t}_\alpha$ and $\underline{t}_{\rm CPA}$ are the single site t-matrices of the component α and of the CPA-medium, respectively. The later quantity is connected with the CPA scattering path operator by an equation analogous to Eq. (78) or (76), respectively. To obtain the quantities $\underline{t}_{\rm CPA}$ and $\underline{\tau}^{nn,{\rm CPA}}$, for given concentrations x_α, one must solve Eqs. (79), (80) and (78) or (76), respectively, iteratively.

3 Applications

3.1 Basic Electronic Properties

Dispersion relations The impact of the spin-orbit coupling on the dispersion relations $E_j(\boldsymbol{k})$ of spin polarized relativistic solids have been investigated by several authors in the past [71,138,155]. Corresponding results for fcc-Ni are shown in Fig. 1 for the magnetization $\boldsymbol{M}$ along the [001]-axis and the wavevector $\boldsymbol{k}$ along the [100]-axis [138]. As one notes, spin-orbit coupling gives rise to a lifting of degeneracies (e.g. at A and B in Fig. 1, left) and causes hybridization or mixing of bands (e.g. at C, D, E and F) that simply cross within a non- or scalar relativistic treatment. In addition, one finds that for Bloch states $|\Psi_{j\boldsymbol{k}}\rangle$ the

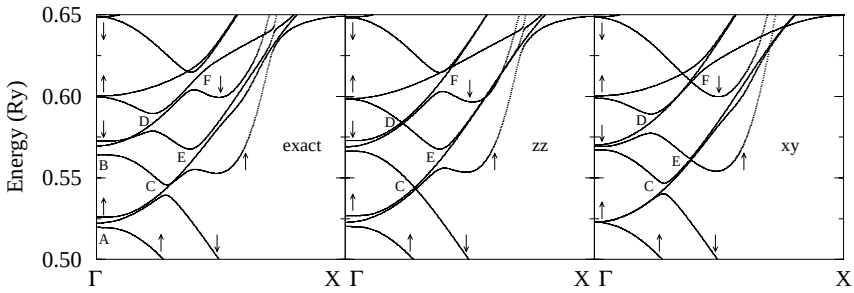

Fig. 1. Dispersion relation $E_j(\boldsymbol{k})$ of fcc-Ni for the magnetization $\boldsymbol{M}$ and the wavevector $\boldsymbol{k}$ along the [001]- and [100]-axis, respectively. The panels show from left to the right results based on the full Dirac equation and those obtained keeping the zz- and xy-terms in Eq. (66).

expectation value $\langle\Psi_{j\boldsymbol{k}}|\sigma_{\rm z}|\Psi_{j\boldsymbol{k}}\rangle$ is not restricted to ±1 (see e.g. Ref. [65,71]), i.e. spin is no more a good quantum number. However, remarkable deviations from the values ±1 occur only in the region where bands cross if spin-orbit coupling is neglected. For this reason it is justified to attach the labels $\downarrow$ and $\uparrow$ to the bands to indicate their dominant spin character for a certain range of $\boldsymbol{k}$.

Keeping only the $\hat{\xi}_{\rm zz}$-part of the spin-orbit interaction the most important consequence is that now all states have pure spin character that cannot change if one goes along a certain band. However, this does not rule out the hybridization of bands induced by $\hat{\xi}_{\rm zz}$. As one can see from the middle panel of Fig. 1 hybridization takes place at E and F. On the other hand, no hybridization is found

at C and D, where now bands of different spin character cross. Furthermore one notes that the splitting of the bands, e.g. at A, B, E and F caused by the $\hat{\xi}_{zz}$-part is quite comparable to that due to the full spin-orbit interaction.

Concerning the hybridization, the situation is more or less opposite to the situation for $\hat{\xi}_{zz}$, if the $\hat{\xi}_{xy}$-part is used. The right panel of Fig. 1 demonstrates that there is now a pronounced hybridization of bands of different spin character (C and D) – just as for the full spin-orbit interaction. While hybridization is also present at E and F, it is much less pronounced than for $\hat{\xi}_{zz}$. Surprisingly, the splitting of the bands caused by $\hat{\xi}_{xy}$, while being in general smaller than for $\hat{\xi}_{zz}$, is still quite appreciable. In spite of this, both parts have a rather different importance for many spin-orbit induced properties, as it will be demonstrated below.

The influence of the spin-orbit coupling on the dispersion relation of ordered spin-polarized solids shown in Fig. 1 can also be demonstrated for disordered ones. Instead via the dispersion relation, the band structure is represented in the later case by means of the Bloch-spectral function $A_{\rm B}(\boldsymbol{k}, E_{\rm F})$ that can be viewed as a $\boldsymbol{k}$-dependent density of states (DOS) function [156]. Due to the chemical disorder, $A_{\rm B}(\boldsymbol{k}, E_{\rm F})$ for a given energy is in general spread out in $\boldsymbol{k}$-space, implying that the wave vector $\boldsymbol{k}$ is not a good quantum number. For an ordered system, on the other hand, the smearing out in $\boldsymbol{k}$-space does not occur and $A_{\rm B}(\boldsymbol{k}, E_{\rm F})$ can be written as a superposition of δ-functions $\delta(E - E_j(\boldsymbol{k}))$ and the conventional dispersion relations are recovered.

Fig. 2 shows results for spin-projected Bloch-spectral function $A_{\rm B}(\boldsymbol{k}, E_{\rm F})$ obtained for fcc-$Fe_{0.2}Ni_{0.8}$ for the Fermi energy $E_{\rm F}$, the wave vector $\boldsymbol{k}$ in the (010)-plane and the magnetization $\boldsymbol{M}$ along the [001]-direction [157]. As one notes, disorder has quite a different impact on the majority and minority spin Bloch-spectral functions. Nevertheless, there is a well-defined Fermi surface for both of them that – due to the specific composition – is very similar to that of pure Ni [26,158]. Comparing the details of the Bloch-spectral function for the two spin sub-systems a hybridization is recognized. This especially holds for the single majority sheet centered at the Γ-point that has a pronounced minority spin admixture. Because the majority spin states primarily carry the electric current [159] and because the spin hybridization leads effectively to a short-cut it should have a great influence on the electric resistivity. In fact, calculations of the isotropic residual resistivity of magnetic alloys using the SPR-KKR-CPA give always higher values than calculations that neglect spin-orbit coupling and make use of the so-called two-current model [160,161].

In addition to the spin hybridization, one notes a small anisotropy of the Bloch spectral function; i.e. it depends on the relative orientation of the wave vector $\boldsymbol{k}$ and the magnetization $\boldsymbol{M}$. This applies not only to the location of $A_{\rm B}(\boldsymbol{k}, E)$ in $\boldsymbol{k}$-space, but also for the width of the Bloch spectral function. The former property is also found for the dispersion relation of ordered systems and clearly indicates the lowered symmetry of the system compared to a paramagnetic state. For the situation considered in Figs. 1 and 2 the symmetry is effectively tetragonal instead of being cubic. Changing the orientation of the

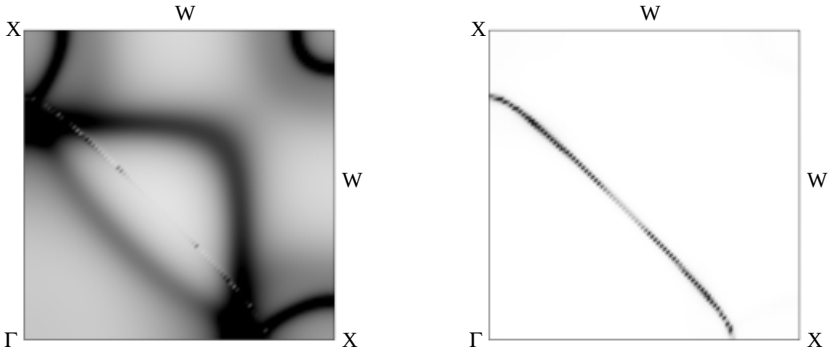

Fig. 2. Gray-scale representation of the Bloch spectral function $A_{\mathrm{B}}(\boldsymbol{k}, E_{\mathrm{F}})$ for fcc-$Fe_{0.2}Ni_{0.8}$ for the energy fixed to the Fermi energy E_{F} and the magnetization $\boldsymbol{M} \parallel [001]$. The wave vector $\boldsymbol{k}$ is in the (010)-plane; i.e. the horizontal axis gives the component of $\boldsymbol{k}$ perpendicular to $\boldsymbol{M}$, while the vertical axis gives that parallel to $\boldsymbol{M}$. The white background corresponds to $A_{\mathrm{B}}(\boldsymbol{k}, E) = 0$, while the black regions represent $A_{\mathrm{B}}(\boldsymbol{k}, E) \geq 50$ a.u.; i.e. the cusps of $A_{\mathrm{B}}(\boldsymbol{k}, E)$ have been cut for a more resolved representation. The left and right parts give the Bloch spectral function decomposed into their minority and majority spin part, respectively.

magnetization $\boldsymbol{M}$ will in general change the symmetry but also the electronic structure itself. The corresponding changes in the total energy give rise to the magneto-striction [162,163] and the magneto-crystalline anisotropy [164,165]. The conventional approach to evaluate magneto-crystalline anisotropy energies is to apply the force theorem [166], that allows to approximate the energy difference for two orientations of the magnetization as the energy difference of the corresponding single particle energies. This means that the small changes found for the dispersion relation when the magnetization is rotated [155,158] are the microscopic origin of the magneto-crystalline anisotropy. In practice the mentioned energy differences are calculated by integrating the various energy-weighted density of states curves or equivalently the integral DOS curves up to a fixed Fermi energy. On the basis of this procedure Újfalussy et al. performed for multilayer systems a layer-wise decomposition of the magneto-crystalline anisotropy energy by using corresponding layer projected DOS functions [167]. Of course, an analogous composition can be made for any multi-component system. Using the KKR-formalism an elegant way to perform the above mentioned energy-integral for the integrated DOS function is to make use of Lloyd's formula [168]. This has recently been used for a calculation of the magneto-crystalline anisotropy energy of disordered fcc-Co_xPt_{1-x} alloys by Razee et al. [169] who also worked out corrections to the expression based on the force theorem.

Finally, it should be emphasized that all calculations of the magneto-crystalline anisotropy energy done so far on the basis of the force theorem or alternative schemes [164,165] account only for the spin-orbit coupling as its microscopic source. The Breit interaction, that gives rise to contributions in the same order

of magnitude, is usually accounted for only in a second step by calculating the so-called shape anisotropy energy [165,170,171].

Charge and Orbital Current Density Distribution For a paramagnetic solid time reversal symmetry implies that spin-orbit coupling viewed as a perturbation leads for states with quantum numbers (m_l, m_s) to the same changes as for $(-m_l, -m_s)$. As a consequence the spatial symmetry of the charge distribution is not affected and no orbital current is induced. For a spin-polarized solid, on the other hand, this does not hold anymore; i.e. states with quantum numbers (m_l, m_s) and $(-m_l, -m_s)$ are affected by the inclusion of the spin-orbit coupling in a different manner because of the exchange splitting. As a consequence the charge distribution will be rearranged according to the lowered symmetry of the system compared to its paramagnetic state. For a magnetic solid with a cubic lattice and the magnetization along the z-axis, for example, the effective symmetry is only tetragonal. Accordingly, self-consistent full-potential spin polarized relativistic calculations lead to non-cubic terms like ρ_{20} and V_{20}, respectively, if for the charge density ρ and the potential V the conventional expansion into spherical harmonics is used [83] (see Eq. (44)).

A further consequence of the presence of the spin-orbit coupling for a spin-polarized solid is that its orbital angular momentum is no more quenched. This corresponds to the occurrence of a finite paramagnetic orbital current density $\boldsymbol{j}_{\mathrm{p}}$ (the adjective paramagnetic can be omitted in the following because external magnetic fields are assumed to be absent; i.e. the physical and paramagnetic current densities are identical).

Within the Green's function formalism used here the current density $\boldsymbol{j}_{\mathrm{p}}$ can be obtained from the expression

$$\boldsymbol{j}_{\mathrm{p}} = -\frac{1}{\pi}\,\mathrm{Trace}\,\Im \int^{E_{\mathrm{F}}} dE\,\frac{1}{\mathrm{i}}[\overrightarrow{\nabla} - \overleftarrow{\nabla}]G(\boldsymbol{r}, \boldsymbol{r}\,', E)|_{\boldsymbol{r}=\boldsymbol{r}\,'}\,. \tag{81}$$

Corresponding results [83] obtained for the current density $\boldsymbol{j}_{\mathrm{p}}$ in bcc-Fe are shown in Fig. 3. Here the direction and magnitude of $\boldsymbol{j}_{\mathrm{p}}$ is represented by arrows for the (001)-plane with the z- and magnetization axes pointing upwards. At first sight the current density distribution seems to be rotational symmetric. However, a closer look reveals that it has in fact a lower symmetry. This is demonstrated in the right part of Fig. 3 which gives the radial component of $\boldsymbol{j}_{\mathrm{p}}$ within the (001)-plane. This component is about 2-3 orders of magnitude smaller than $\boldsymbol{j}_{\mathrm{p}}$ itself and has been scaled by a factor of approximately 350 with respect to the left part of Fig. 3. As one notes, there is only a four-fold symmetry axis along the z-axis. For the paramagnetic state the x- and y-axes as well as the diagonal axes in between would be twofold symmetry axes. Obviously, the corresponding symmetry operation C_2 is missing here because of the ferromagnetic state and the spin-orbit coupling accounted for. However, one can also clearly see from the right part of Fig. 3 that this symmetry operations combined with the time reversal operator T result in proper symmetry operations $(TC_{2\perp})$ for the ferromagnetic state [144].

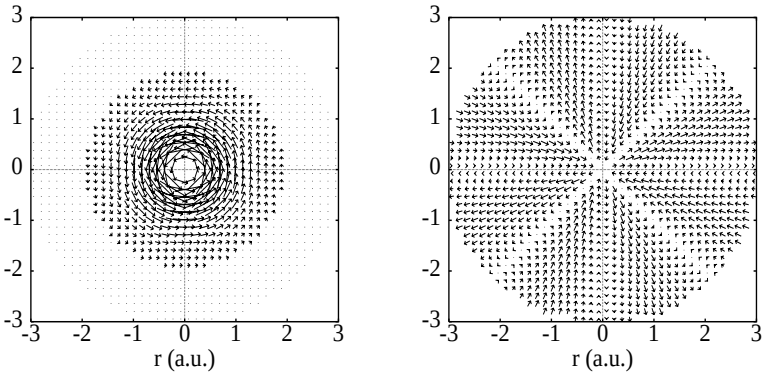

Fig. 3. Orbital current density $\boldsymbol{j}_{\rm p}$ for bcc-Fe in the (001)-plane (left). The right part gives the corresponding radial component scaled by a factor of around 350 with respect to the left part. For display $\boldsymbol{j}_{\rm p}$ has been weighted with r^2.

3.2 Orbital Magnetic Moments

With the spin-orbit-induced orbital current density in magnetic solids there is obviously a finite orbital angular momentum density associated. For a rotational symmetric current density distribution, for example, one has circular currents implying the simple relationship [83]

$$\langle \beta l_{\rm z}(\boldsymbol{r}) \rangle = \frac{1}{2\sqrt{2}} \langle r j_{{\rm p},\phi}(\theta, r) \rangle \ , \tag{82}$$

where $j_{{\rm p},\phi}$ is the ϕ-component of $\boldsymbol{j}_{\rm p}$ that gives its magnitude along a closed circular loop.

Connected with $\langle \beta l_{\rm z} \rangle$ there is of course a corresponding orbital magnetic moment $\mu_{\rm orb}$ that can be obtained via Eq. (82) or directly from the conventional expression [24,83]:

$$\mu_{\rm orb} = -\frac{\mu_{\rm B}}{\pi} {\rm Trace}\, \Im \int^{E_{\rm F}} dE \int d^3r \, \beta l_{\rm z} G(\boldsymbol{r}, \boldsymbol{r}, E) \ . \tag{83}$$

As Fig. 4 shows, the spin-orbit induced $\mu_{\rm orb}$ contributes 5 to 10 % of the total magnetic moments of the elemental ferromagnets Fe, Co and Ni. However, one also notes from this figure that the results obtained on the basis of plain SDFT are much too small compared with experiment in the case of Fe and Co. To cure this problem, that also occurs for f-electron systems, Brooks introduced the OP-formalism [113], that was originally restricted to $\boldsymbol{k}$-space band structure methods. Using the real-space formulation given above, one can see that it effectively leads to a feed-back of the spin-orbit induced orbital current into the potential term of the Dirac equation (see Eq. (19)). Based on the corresponding spin- and orbital polarized relativistic (SOPR) KKR-formalism [118], one finds a strong enhancement of the orbital magnetic moment for Fe and Co leading to

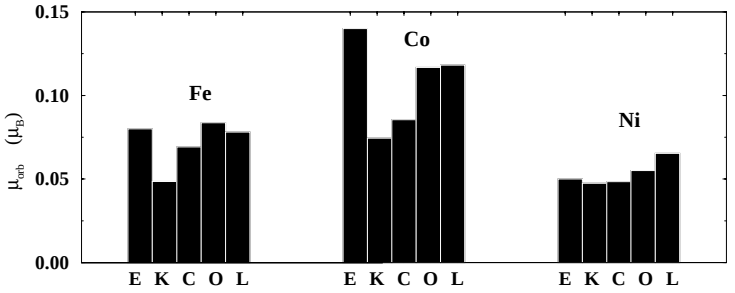

Fig. 4. Orbital magnetic moments for bcc-Fe, fcc-Co and fcc-Ni. The various columns represent from left to right the experimental data (E) [172] and the theoretical data obtained by the plain SPR-KKR- (K), within CDFT (C) [109] as described in the text as well as the SOPR-KKR (O) [118] including the OP-potential term. The last column labeled with L gives results obtained using the LMTO that account for spin-orbit coupling and the OP-term in the variational step [51,173].

a rather satisfying agreement with experiment (see Fig. 4). The spin magnetic moment, on the other hand, is hardly affected by inclusion of the OP-term. Furthermore, calculations done in the full-potential mode [83] clearly demonstrated that the OP-term does not include aspherical potential terms that would be accounted twice in a full-potential calculation, as it was sometimes suspected in the past.

Apart from minor numerical differences, the results obtained with the SOPR-KKR are completely in line with those obtained before using the LMTO-method [51,173,174]. However, the latter approach accounts for spin-orbit coupling and the OP-term only in the variational step, while for the SOPR-KKR these are also included when calculating the wave functions and the corresponding single-side t-matrices. As a consequence the SOPR-KKR can straightforwardly be combined with the CPA to deal with disordered alloys. As an example for an application of the SOPR-KKR-CPA results for $\mu_{\rm orb}$ of bcc-Fe_xCo_{1-x} are shown in Fig. 5 [118].

In contrast to the investigations of Söderlind et al. [175] done using the LMTO together with the virtual crystal approximation (VCA) alloy theory [156] the SOPR-KKR-CPA supplies component-resolved results. As one can see in Fig. 5 the enhancement of $\mu_{\rm orb}$ for Fe and Co in bcc-Fe_xCo_{1-x} are very similar to that found for the pure metals. Again this enhancement brings the average orbital magnetic moment for the alloy in very satisfying agreement with experiment.

Because the OP-term is very similar in form to the operator representing spin-orbit coupling as a correction or perturbation, one may expect that it will not only affect the spin-orbit induced orbital magnetic moments but also any other quantity caused by spin-orbit coupling. This is in general indeed the case as it could be demonstrated by investigations on the spin-orbit induced band-splittings [176], the orbital contributions to the hyperfine fields [118], the magneto-crystalline anisotropy [177], galvano-magnetic properties [178], the

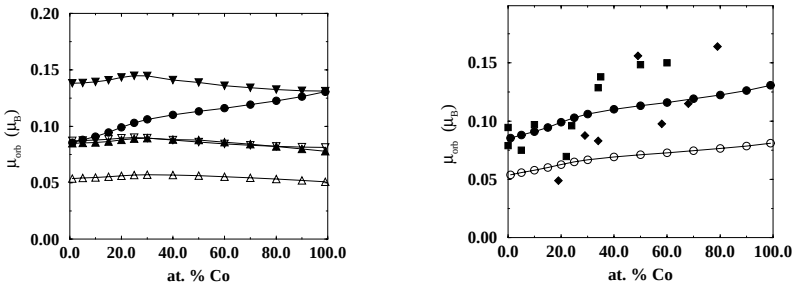

Fig. 5. Orbital magnetic moments in bcc-Fe_xCo_{1-x}. The triangles pointing up- and downwards represent the theoretical moments of Fe and Co, respectively, while the concentration weighted sum is given by circles. Full and open symbols stand for results obtained with and without the OP-term included (SOPR- and SPR-KKR-CPA, resp.). Experimental data [172] for the average magnetic moment (right part) stemming from magnetomechanical and spectroscopic g-factors are given by full squares and diamonds.

magneto-optical Kerr effect [179] and the magnetic dichroism in X-ray absorption [180].

Using the OP-formalism, one obviously leaves the framework of density functional theory and arrives at a heuristic hybrid scheme. From a formal point of view CDFT therefore supplies a much more satisfying basis to deal with orbital magnetism. Results for $\mu_{\rm orb}$ of Fe, Co and Ni, that have been obtained using the relativistic version of Vignale and Rasolt's CDFT-formalism, are given in Fig. 4 [109]. Obviously using CDFT instead of plain SDFT leads indeed to an enhancement of $\mu_{\rm orb}$ for Fe and Co. Although this effect is found to be too small, one may expect that the remaining deviation from experiment will be reduced with improved parameterizations for the exchange-correlation potentials available.

The basic CDFT-Hamiltonian in Eq. (14) does not rule out the existence of a finite orbital magnetic moment in the non-relativistic limit. With the help of model calculations, it could be demonstrated that this is not the case [109]. Starting a SCF-calculation with a finite spin-orbit induced orbital current density and switching off the spin-orbit coupling during the SCF-cycle the orbital magnetic moment vanished.

Using Vignale and Rasolt's formulation of CDFT [104,105], one has to use the current density in a spin-projected way. This leads to quite large contributions in the nucleus near region stemming from the core states, that essentially cancel if the spin contributions are summed up (see for example Fig. 3). However, for transition metals the corresponding core contributions to the exchange-correlation potential $\boldsymbol{A}_{{\rm xc},\sigma}(\boldsymbol{r})$ has not much overlap with the current density of the valence d-electrons. Because $\mu_{\rm orb}$ stems primarily from these, the core contribution to $\boldsymbol{A}_{{\rm xc},\sigma}(\boldsymbol{r})$ can be neglected. For bcc-Fe the corresponding valence band part of the polar component of the spin-dependent exchange-correlation vector potential $\boldsymbol{A}_{{\rm xc},\sigma}(\boldsymbol{r})$ is given in Fig. 6 (left part). Because the OP-term can be manipulated to represent a coupling to the electronic orbital degree of freedom or current,

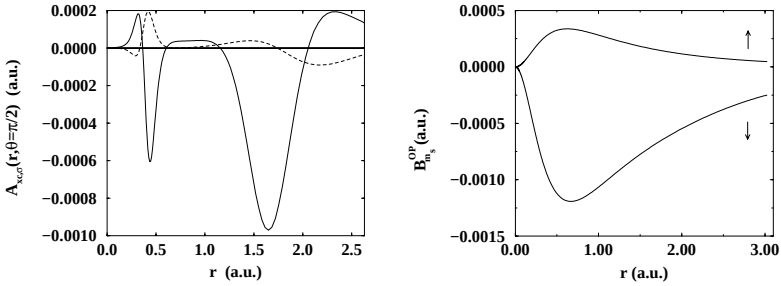

Fig. 6. Left: Valence band part of the polar component of the spin-dependent exchange-correlation vector potential $\boldsymbol{A}_{\mathrm{xc},\sigma}(r,\theta)$ for bcc-Fe (in atomic units). The full and dashed lines give the potential for minority and majority character, respectively, for $\theta = \pi/2$. Right: The OP potential term B_σ^{OP} for bcc-Fe as calculated by the self-consistent FP-OP-SPR-KKR.

respectively, a corresponding vector potential function B_σ^{OP} can be constructed within the OP-formalism [83]. However, one has to keep in mind that the physical picture behind the OP-formalism is quite different from the CDFT as used here. While for the former case one tries to account in an approximate way for intra-atomic correlations, the vector potential occurring within CDFT is due to diamagnetic contributions to the exchange-correlation energy of the electron gas. Accordingly, it is not surprising that the resulting vector potential function (see Fig. 6) for the OP-formalism is quite different from that obtained within CDFT. In spite of this fundamental difference one finds the current density $\boldsymbol{j}_{\mathrm{p},\sigma}$ calculated within the extended OP-formalism to be very similar to that calculated within the framework of CDFT [83], i.e. both differ only with respect to their absolute magnitude but not concerning their radial variation. For this reason, the OP-formalism, that is extremely simple to be implemented, may be used to study the influence of corrections to the exchange-correlation energy due to finite orbital currents as long as no better parameterizations for this have been derived within CDFT.

3.3 Hyperfine Interaction

Quadrupolar Hyperfine Interaction The nuclear quadrupolar hyperfine interaction, that can be investigated experimentally, for example, by means of Mößbauer spectroscopy or NMR, denotes the coupling of the nuclear quadrupole moment Q with the electric field gradient (EFG) stemming from the surrounding electronic charge distribution. Because the nuclear quadrupolar hyperfine interaction reflects the local site-dependent symmetry of the charge and potential distribution in a rather direct way, it provides a unique tool to investigate the consequence of the spin-orbit coupling for the symmetry of a spin-polarized cubic solid.

The electric field gradient, that is only non-zero for a site-symmetry lower than cubic, can be calculated straightforwardly from the Coulomb part of the

electronic potential V. Expanding V into spherical harmonics (see Eq. (44)) one has, for example, for the zz-component of the electric field gradient tensor [181]:

$$\Phi_{zz} = eq = 2 \lim_{r \to 0} V_{20}(r) \; . \tag{84}$$

As an alternative, the EFG can also be calculated from the corresponding non-spherical charge distribution term $\rho_{20}(r)$ within the central Wigner-Seitz cell and a Madelung contribution stemming from the multipoles on the neighboring sites [130,146,181].

For the case that the electric field gradient is caused by the low symmetry of the underlying lattice it was found in the past that it is often sufficient to perform self-consistent calculations for the charge density only in the spherical approximation and to determine the non-spherical charge density $\rho_{lm_l}(r)$ only in the final iteration (spherical approximation). In addition it was found from FP-SPR-KKR calculations on Fe that the spin-orbit induced electric field gradient stems nearly exclusively from the non-spherical charge density within the central cell containing the nucleus while the contribution of the surrounding can be ignored [146]. Using these simplifications together with the ASA-version of the SPR-KKR formalism the electric field gradient tensor component Φ_{zz} can be written as [139]:

$$\Phi_{zz} = \frac{8\pi}{5} \int_0^S \frac{\rho_{20}(r)}{r} \, dr \tag{85}$$

$$= \frac{8\pi}{5} e \frac{-1}{\pi} \Im \int dE \sum_{\Lambda\Lambda'} \tau_{\Lambda\Lambda'} \sum_{\Lambda''\Lambda'''} \tag{86}$$

$$\Big[B_{\Lambda''\Lambda'''} \int_0^S \frac{g_{\Lambda''\Lambda} \, g_{\Lambda'''\Lambda'}}{r} dr + B_{-\Lambda''\,-\Lambda'''} \int_0^S \frac{f_{\Lambda''\Lambda} \, f_{\Lambda'''\Lambda'}}{r} dr \Big] \; .$$

with the angular matrix elements $B_{\Lambda\Lambda'}$ given by

$$B_{\Lambda\Lambda'} = \delta_{\mu\mu'} (-1)^{\mu - 1/2} \frac{\sqrt{(2l+1)(2l'+1)}}{4\pi} \, C(ll'2; 00) \sum_{m_s} C_{\Lambda}^{m_s} C_{\Lambda'}^{m_s} C(ll'2; (\mu - m_s)(-\mu + m_s)) \tag{87}$$

and the Clebsch Gordon coefficients $C(l\tfrac{1}{2}j; (\mu - m_s)m_s)$ represented by the short hand notation $C_{\Lambda}^{m_s}$.

This approach has been used to study the properties of 5d-transition metal impurities dissolved substitutionally in bcc-Fe [182]. These impurity type calculations have been done in the single-site approximation ignoring the distortion of Fe-atoms in the vicinity of the impurity. The resulting electric field gradient parameter $q = \Phi_{zz}/e$ is shown in Fig. 7 for the whole 5d-series. First of all one notes that q is only around one order of magnitude smaller than that usually found for a lattice-induced EFG [187]. Taking into account that the existing experimental data are scattering quite strongly and that measurements on single crystals with a definite relative orientation of the magnetization and the crystal

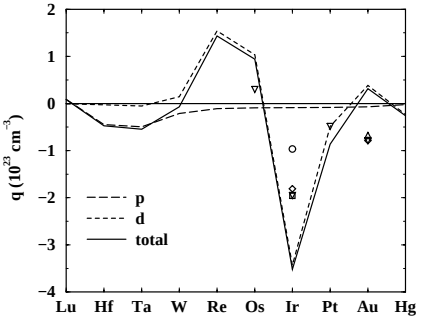

Fig. 7. EFG parameter q of 5d-transition metal-impurities in Fe. Theoretical results for the magnetization direction along the z-axis together with their decomposition into p- and d-electron contributions are given by full, dotted and dashed lines, respectively. Experimental data stem from powder as well as from single crystal measurements [183–186].

axis were done only in some few cases, agreement of the theoretical results with experiment is quite satisfying. In particular the pronounced dip of the EFG as a function of the ordering number Z for Ir seems to be confirmed by experiment. The variation found for q as a function of Z strongly resembles that obtained earlier for the spin-orbit induced contributions to the magnetic hyperfine field [188], which are predominantly of orbital origin. Earlier, more qualitative investigations [189,190] assumed that this contribution is exclusively due to the d-electrons. However, it turned out that the p-electrons contribute to a similar extent to the magnetic hyperfine field showing only a weak variation with Z [188]. A similar situation is encountered here for the EFG parameter q. As can be seen in Fig. 7 the p-electrons contribute in particular for the early 5d-transition metals, where they exceed the d-electron contribution. Nevertheless, one also notes that the variation of q with Z is primarily due to its d-electron part.

Based on perturbation theory it was expected that the spin-orbit induced EFG should depend quadratically on the spin-orbit coupling strength [184]. Using the manipulation scheme described in section 2.2 this could be verified for the d-electron contribution, while for the p-electrons a pronounced deviation from the quadratic dependency has been found. So far it has been assumed that the spin-orbit induced EFG stems predominantly from the spin-diagonal part ξ_{zz} of the spin-orbit coupling (see Eq. (66)). However, performing corresponding model calculations it was found that the spin-mixing part ξ_{xy} contributes to the same order of magnitude but with opposite sign.

Because the EFG reflects the local symmetry one expects it to change with the orientation of the magnetization; i.e. it should monitor the fact that the spin-orbit induced anisotropy is anisotropic. This could indeed be demonstrated

recently by Seewald et al. [46], who determined the EFG of Ir in bcc-Fe for the magnetization pointing along the [001]-, [111]- and [110]-directions. It is interesting to note that this type of anisotropy was too weak to be detected in the case of magneto-optical Kerr effect (MOKE) investigations on fcc-Co [191,192].

Magnetic Hyperfine Interaction The magnetic hyperfine interaction represents the interaction of the nuclear magnetic moment $\boldsymbol{\mu}_{\mathrm{n}}$ with the current density $\boldsymbol{j}$ of the surrounding electronic system. In its relativistic form the corresponding operator $\mathcal{H}_{\mathrm{hf}}$ is given by [7,193]:

$$\mathcal{H}_{\mathrm{hf}} \;=\; ec\boldsymbol{\alpha} \cdot \boldsymbol{\mu}_{\mathrm{n}} \times \boldsymbol{r}/r^3 \;. \tag{88}$$

Here only the static part of the hyperfine interaction is considered. Assuming the magnetization and quantization axis to point along the z-axis, only the part $\mathcal{H}_{\mathrm{hf,z}} \propto \alpha_{\mathrm{z}}(\boldsymbol{\mu}_{\mathrm{n}} \times \boldsymbol{r})_{\mathrm{z}}$ has to be accounted for.

Within a non-relativistic theoretical description of the hyperfine interaction it is conventional to split the total hyperfine interaction operator into three distinct contributions: the Fermi-contact, the spin-dipolar and the orbital terms. While the first is relevant only for s-electrons, the other two are connected exclusively to non-s-electrons. Starting from a Gordon-decomposition of the electronic current, a corresponding decomposition of the hyperfine interaction operator $\mathcal{H}_{\mathrm{hf}}$ in Eq. (88) can also be made within relativistic theory [139,182,194]. For the orbital part one gets for example the expression:

$$\mathcal{H}_{\mathrm{hf,orb}} = 2\mu_{\mathrm{B}}\beta\boldsymbol{\mu}_{\mathrm{n}}\boldsymbol{l} \cdot \begin{cases} r^{-3} \text{ for } r > r_{\mathrm{n}} \\ r_{\mathrm{n}}^{-3} \text{ for } r < r_{\mathrm{n}} \end{cases} , \tag{89}$$

where r_{n} is the nuclear radius. This expression already indicates that for the decomposition of the relativistic hyperfine interaction operator a nucleus of finite size has to be considered [182,194]. Furthermore one has to note that the various parts of $\mathcal{H}_{\mathrm{hf}}$ are no more exclusively due to s- or non-s-electrons, respectively.

For spontaneously magnetized solids the central hyperfine interaction parameter is the hyperfine field B_{hf}. This quantity is determined by the expectation value of the static part of the hyperfine interaction operator:

$$B_{\mathrm{hf}} = \langle \mathcal{H}_{\mathrm{hf,z}} \rangle / \hbar\gamma_{\mathrm{n}} \;, \tag{90}$$

with γ_{n} the nuclear gyromagnetic ratio. Representing the underlying electronic structure by means of the Green's function formalism $\langle \mathcal{H}_{\mathrm{hf,z}} \rangle$ in turn is given by [24]:

$$\langle \mathcal{H}_{\mathrm{hf,z}} \rangle \;=\; -\frac{1}{\pi}\,\mathrm{Trace}\,\Im \int dE \int d^3r\, \mathcal{H}_{\mathrm{hf,z}}(\boldsymbol{r})\, G(\boldsymbol{r}, \boldsymbol{r}, E) \;. \tag{91}$$

Dealing with this expression on a non-relativistic level one gets contributions to the hyperfine field B_{hf} only from the Fermi-contact and spin-dipolar terms

because the orbital magnetization density is quenched in the solid [109] (see above). Contributions due to the spin-dipolar term are in general ignored because they arise only from a non-cubic electronic spin density distribution. For these reasons the standard approach to calculate hyperfine fields is to determine just its Fermi-contact contribution stemming from s-electrons. In contrast to this simple but conventional approach, the fully relativistic scheme given above leads to contributions to the hyperfine field from non-s-electrons as well. These are caused by the spin-orbit coupling and are non-negligible even for cubic systems [25].

The left part of Fig. 8 shows the total hyperfine fields of Fe in fcc-Fe_xPd_{1-x} together with a decomposition into contributions stemming from the core, valence and non-s-electrons. The experimental data available for Fe indicate that

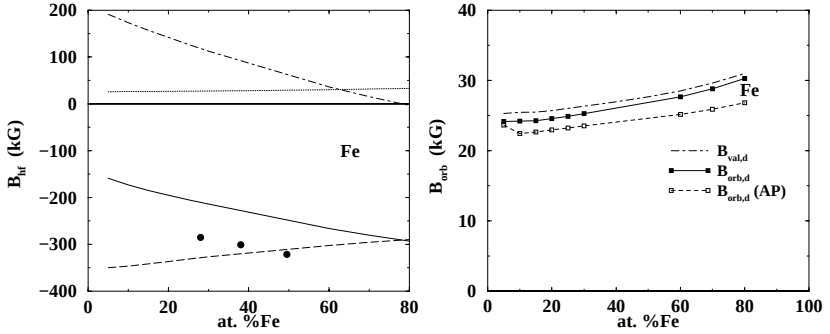

Fig. 8. Left: Hyperfine fields of Fe in fcc-Fe_xPd_{1-x}. In addition to the total field $B_{\rm hf}$ (total) the contributions of the core, valance and non-s-electrons are given separately. Available experimental data have been added. Right: Contributions $B_{\rm val}$ of the d-like valence electrons to the hyperfine fields of Fe in fcc-Fe_xPd_{1-x}. The fields $B_{\rm orb}$ represent the corresponding orbital part. This has also been determined by the approximation due to Abragam and Pryce (AP, see Eq. (3.3)) [195].

the theoretical fields are too small in magnitude. Discrepancies similar to these have been found before for many other systems and have been ascribed to problems in dealing with the core polarization contribution when the spin density functional theory is used on a local-density approximation (LDA) level [20,24]. However, improvements to the LDA, like the generalized gradient approximation (GGA) [196] or the self-interaction correction (SIC) [196,125] did not give much better results. Using the optimized effective potential (OEP), on the other hand, very satisfying results for the hyperfine fields of Fe, Co and Ni could be achieved recently [197].

Within a non-relativistic calculation of the hyperfine fields in Fe_xPd_{1-x} one would get only contributions due to the s-electrons via the Fermi-contact interaction. Within a fully relativistic investigation this part is enhanced by about 10% for Fe [25]. In addition one finds quite appreciable contributions from non-

s-electrons. These are induced by the spin-orbit coupling and in general opposite to the normally dominating negative core polarization fields.

The dominating part of the non-s-fields stemming from the valence band electrons is given once more in Fig. 8 (right part). For Fe this stems nearly exclusively from the d-electrons. With the proper relativistic decomposition of the hyperfine interaction in Eq. (88), the origin of these fields can be investigated in a detailed way. The corresponding fields $B_{\mathrm{orb,d}}$ obtained using the relativistic orbital hyperfine interaction operator (see Eq. (89)) have been added to Fig. 8. As one can see these fields differ only slightly from $B_{\mathrm{val,d}}$ implying that the fields coming from d-electrons via the Fermi-contact and spin dipolar interaction are in general negligible. This is also confirmed by an additional and direct calculation of these fields. For this reason it is quite well justified to call the spin-orbit induced hyperfine fields coming from non-s-electrons in a somewhat loose way *orbital* [25].

One of the most important consequences of the spin-orbit coupling for magnetic solids is the presence of a spin-orbit induced orbital electronic current density that gives rise – according to Eq. (89) – to the orbital hyperfine fields but that causes also a corresponding orbital contribution μ_{orb} to the total magnetic moment. Because of their common physical origin one can expect the fields B_{orb} and the moment μ_{orb} to be related via [195]:

$$B_{\mathrm{orb},l} \;=\; 2\mu_{\mathrm{B}} \left\langle r^{-3} \right\rangle \mu_{\mathrm{orb},l} \quad (l = p, d) \; .$$

As it can be seen in Fig. 8, this simple approximation works quite well justifying once more the designation *orbital* used above.

3.4 Linear Response

Static Magnetic Susceptibility and Knight Shift Using the Green's function formalism for a description of the underlying electronic structure gives several important advantages when dealing with response quantities. In the case of the static magnetic susceptibility, for example, it is straightforward that way to deal with inhomogeneous systems. This has been demonstrated among others by Terakura et al. [198], who calculated the non-local site-dependent susceptibility χ^{ij} of several paramagnetic transition metals. A corresponding relativistic approach has been worked out by Staunton [199] that has been applied to pure transition metals [200,201] with fcc and hcp structure, respectively. The first step of this approach is to use the first order-approximation to the Dyson equation to represent the Green's function G^B of the investigated system in the presence of an external magnetic field B_{ext} in terms of the Green's function G of the unperturbed system:

$$\begin{aligned} G^B(\boldsymbol{r}, \boldsymbol{r}\,', E) = G(\boldsymbol{r}, \boldsymbol{r}\,', E) + \\ \int d^3r'' G(\boldsymbol{r}, \boldsymbol{r}\,'', E) \mathcal{H}^{\mathrm{spin}}_{\mathrm{pert}}(\boldsymbol{r}\,'') G(\boldsymbol{r}\,'', \boldsymbol{r}\,', E) \; . \end{aligned} \tag{92}$$

Within the framework of SDFT the perturbing Hamiltonian $\mathcal{H}^{\rm spin}_{\rm pert}$ is given by [199–201]:

$$\mathcal{H}^{\rm spin}_{\rm pert} = \sigma_{\rm z}[2\mu_{\rm B}B_{\rm ext} - (V^{\uparrow}_{\rm xc} - V^{\downarrow}_{\rm xc})] \; . \tag{93}$$

Here the second term represents a feedback of the induced spin-magnetization via the modified exchange and correlation potentials $V^{\uparrow(\downarrow)}$ that gives rise to the Stoner enhancement mechanism [202]. The spin susceptibility $\chi_{\rm spin}$ is obtained from Eqs. (92) and (93) by calculating the expectation value of the operator $\beta\sigma_{\rm z}$ and eliminating the external field $B_{\rm ext}$ [199]:

$$\chi_{\rm spin} = -\frac{\mu_{\rm B}}{\pi B_{\rm ext}} \, {\rm Trace} \, \Im \int dE \int d^3r \, \beta\sigma_{\rm z} \, G^B(\boldsymbol{r}, \boldsymbol{r}, E) \; . \tag{94}$$

The procedure sketched here is not restricted to calculations of the spin susceptibility but has a much broader range of application. First of all one has to note that the perturbing Hamiltonian in Eq. (93) represents just the coupling of the external magnetic field to the spin of the electrons. In addition, there is a coupling to the orbital degree of freedom. Within a non-relativistic treatment this gives rise to the diamagnetic Langevin and Landau susceptibilities and the paramagnetic VanVleck susceptibility [203,204]. A straightforward way to obtain the later contribution in a fully relativistic way is to replace the operator $\chi^{\rm spin}_{\rm pert}$ in Eq. (93) by:

$$\mathcal{H}^{\rm orb}_{\rm pert} = 2\mu_{\rm B} l_{\rm z} B_{\rm ext} \tag{95}$$

and replacing $\sigma_{\rm z}$ by $l_{\rm z}$ in Eq. (94) giving the VanVleck susceptibility $\chi_{\rm VV}$ instead of $\chi_{\rm spin}$. Here it has to be noted that the standard non-relativistic treatment of the spin- and orbital magnetic susceptibility do not lead to any spin-orbital cross terms. Within a fully relativistic treatment, on the other hand, the perturbing Hamiltonian $\mathcal{H}^{\rm spin}_{\rm pert}$ in Eq. (93) will lead to a non-vanishing orbital susceptibility due to the spin-orbit coupling; i.e. replacing $\sigma_{\rm z}$ by $l_{\rm z}$ in Eq. (94) for $\chi_{\rm spin}$ will give an orbital contribution in addition to the pure spin susceptibility $\chi_{\rm spin}$. Analogously, calculating the expectation value of $\beta\sigma_{\rm z}$ with the orbital perturbation Hamiltonian $\mathcal{H}^{\rm orb}_{\rm pert}$ in Eq. (94) will give rise to a spin contribution in addition to the pure orbital VanVleck susceptibility. The remaining contribution to the orbital susceptibility – the Langevin and Landau susceptibilities – can also be treated in a fully relativistic way by a corresponding extension of the non-relativistic theory [203].

A quantity that is closely connected to the susceptibility is the Knight shift that gives the ratio of the induced hyperfine field $B_{\rm hf}$ seen by a nucleus and the external inducing magnetic field. Using the linear response formalism sketched above one has [25,205]:

$$K = -\frac{1}{\pi}\frac{1}{\hbar\gamma_{\rm n}B_{\rm ext}} \, {\rm TrIm} \int dE \int d^3r \, \mathcal{H}_{\rm hf,z}(\boldsymbol{r}) \, G(\boldsymbol{r}, \boldsymbol{r}, E) \tag{96}$$

where $\mathcal{H}_{\rm hf,z}$ is the z-part of the relativistic hyperfine interaction Hamiltonian (see Eq. (88)). Making use of the Gordon decomposition of the electronic current

density, K can be decomposed into the conventional Fermi-contact, the spin dipolar and the orbital part.

So far, there are only very few theoretical investigations on the Knight shift in transition metal systems that can be found in the literature. Very similar to the situation for the hyperfine field of spontaneously magnetized solids nearly all of these considered only the Fermi contact interaction due to the s-electrons. Using a non-relativistic version of the linear response formalism presented above, the first calculation of all contributions to the Knight shift has been done for the transition metals V, Cr, Nb and Mo [206]. For these metals the VanVleck contribution to the magnetic susceptibility and to the Knight shift was found to be of the same order of magnitude as the various spin contributions and to stem nearly exclusively from the d-electrons. Concerning the magnetic susceptibility similar results have been obtained by Yasui and Shimizu using a non-relativistic [207] as well as fully relativistic [208] approach.

Results obtained using the above relativistic linear response formalism are given in Fig. 9. The left panel of this figure shows the VanVleck susceptibility

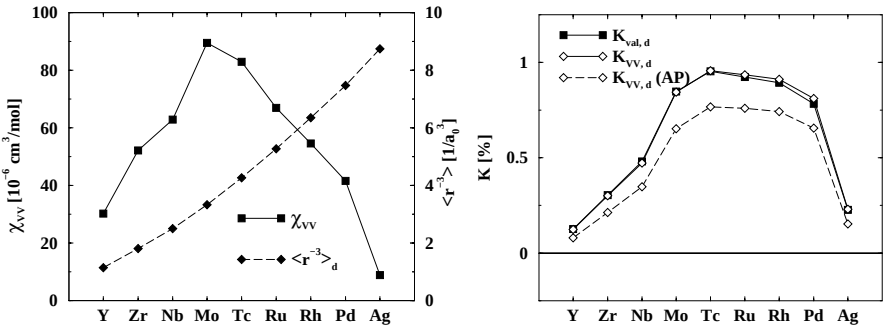

Fig. 9. VanVleck susceptibility χ_{VV} (left), expectation value of r^{-3} (left) and VanVleck contribution to the Knight shift K_{VV} (right) for the d-valence band electrons of the pure 4d-transition metal elements. The estimation for K_{VV} based on the approximation proposed by Abragam and Pryce (AP) as well as the total valence contribution K_{val} due to the orbital perturbation term $\mathcal{H}^{\mathrm{orb}}_{\mathrm{pert}}$ in Eq. (95) has been added (right).

χ_{VV} of the pure 4d-transition metals. As found within earlier studies a maximum is present for χ_{VV} roughly in the middle of the row. This can be explained by using a simplified expression for χ_{VV} [209] and the fact that here the product $n_{\mathrm{o}} \cdot n_{\mathrm{u}}$ of the number of occupied (n_{o}) and unoccupied (n_{u}) d-states is at its maximum. From the relationship of the orbital parts of the magnetic moment and the hyperfine field (see Eq. (3.3)) one can expect an analogous relationship for the VanVleck contributions to the susceptibility and Knight shift:

$$K_{\mathrm{VV},l} \;=\; 2\mu_{\mathrm{B}} \left\langle r^{-3} \right\rangle \chi_{\mathrm{VV},l} \quad (l = p, d) \; . \tag{97}$$

As one can see in Fig. 9 (left) the expectation value $\langle r^{-3} \rangle_{\rm d}$ for the 4d-elements increases rapidly along the 4d row. The reason for this is that the corresponding d-like wave function gets more and more localized with increasing atomic number. Combining the results for $\chi_{\rm VV}$ and $\langle r^{-3} \rangle_{\rm d}$ using Eq. (97) leads to an estimate for the VanVleck Knight shift $K_{\rm VV}$ that is shown in Fig. 9 (right). Due to the variation of $\langle r^{-3} \rangle_{\rm d}$ the maximum in $K_{\rm VV}$ is obviously shifted to the right compared with the $\chi_{\rm VV}$ curve. Fig. 9 shows in addition the shift $K_{\rm VV}$ that has been obtained by the full formalism; i.e. Eqs. (89), (92), (95), and (96). As one can see the estimation of $K_{\rm VV}$ using $\chi_{\rm VV}$ and $\langle r^{-3} \rangle_{\rm d}$ reproduces the variation with atomic number quite well. However, in line with previous non-relativistic results [206], the absolute values differ by up to about 20%. This means that estimations based on Eq. (97) are in general less reliable than spin-orbit induced orbital hyperfine fields estimated using Eq. (3.3).

Finally, it should be emphasized that the VanVleck Knight shift $K_{\rm VV}$ given in Fig. 9 stems from the coupling of the external magnetic field to the orbital degree of freedom (see Eq. (95)). Because of the use of the relativistic orbital hyperfine interaction operator (see Eq. (89)) it is by definition of pure orbital nature. If the full hyperfine interaction operator (Eq. (88)) is used instead, the Knight shift denoted $K_{\rm val}$ in Fig. 9 is obtained. The small difference between $K_{\rm VV}$ and $K_{\rm val}$ is of pure spin nature. Within a non-relativistic formalism this cross contribution cannot be accounted for, because it is a consequence of spin-orbit coupling.

This section is somewhat outside the main issue of this review, because it presents results for paramagnetic solids. However, one should notice that the formalism presented above can be applied without modifications to deal with the high-field susceptibility of spontaneously magnetically ordered solids, as well as the Knight shift in such systems. Furthermore, one can apply the linear response formalism also to deal with magneto-crystalline anisotropy or the various kinds of spin-spin coupling constants [168,210].

Transport properties A further interesting application of the linear response formalism is the treatment of galvano-magnetic properties of disordered alloys. Here the Kubo-Greenwood formalism allows one to express the elements of the electrical conductivity tensor $\boldsymbol{\sigma}$ in terms of a current-current correlation function [211,212]:

$$\sigma_{\mu\nu} = \frac{\hbar}{\pi V_{\rm cryst}} {\rm Tr} \left\langle j_\mu \, \Im \, G^+(E_{\rm F}) \, j_\nu \, \Im \, G^+(E_{\rm F}) \right\rangle_{\rm conf.} , \tag{98}$$

where j_μ is the μth spatial component of the electronic current density operator $\boldsymbol{j} = ec\boldsymbol{\alpha}$. In the following it is assumed that a finite conductivity or resistivity, respectively, of the investigated system stems exclusively from chemical disorder, i.e. contributions caused by lattice imperfections, grain boundaries, phonons, magnons, and so on are ignored. This implies in particular that one is dealing

with the residual resistivity and that $\langle \cdots \rangle_{\text{conf.}}$ in Eq. (98) denotes the atomic configuration average for a disordered alloy.

For a paramagnetic cubic solid the conductivity tensor that results from Eq. (98) is diagonal with all elements identical, i.e. the conductivity is isotropic. For a ferromagnetic cubic solid, however, this is not the case and the form of the conductivity tensor depends on the direction of the magnetization reflecting the lowered symmetry of the system. A very general procedure to work out the corresponding symmetry properties of response functions has been developed by Kleiner [213] (for a somewhat alternative approach, see for example Ref. [214]). For example, for a cubic solid with the magnetization along the z-axis one finds that way the form [215]:

$$\boldsymbol{\rho} = \boldsymbol{\sigma}^{-1} = \begin{pmatrix} \rho_\perp & -\rho_{\text{H}} & 0 \\ \rho_{\text{H}} & \rho_\perp & 0 \\ 0 & 0 & \rho_\parallel \end{pmatrix} . \tag{99}$$

Here $\boldsymbol{\rho}$ is the resistivity tensor with $\rho_\perp$ and $\rho_\parallel$ the transverse and longitudinal resistivities, respectively, and ρ_{H} the spontaneous or anomalous Hall resistivity. In addition one defines the spontaneous magnetoresistance anisotropy (SMA) or anomalous magnetoresistance (AMR) ratio by [215]:

$$\frac{\Delta\rho}{\bar{\rho}} = \left. \frac{\rho_\parallel(B_{\text{ext}}) - \rho_\perp(B_{\text{ext}})}{\bar{\rho}(B_{\text{ext}})} \right|_{B_{\text{ext}} \to 0} , \tag{100}$$

where $\bar{\rho} = \frac{1}{3}(2\rho_\perp + \rho_\parallel)$ is the isotropic resistivity. Here the notation emphasizes that experimentally the SMA is determined by measuring $\rho_\parallel(B_{\text{ext}})$ and $\rho_\perp(B_{\text{ext}})$ as a function of an applied external magnetic field B_{ext} and extrapolating to $B_{\text{ext}} = 0$. The reason for this is that in contrast to investigations on the conventional magnetoresistance $\Delta\rho/\rho = (\rho(B_{\text{ext}}) - \rho(0))/\rho(0)$ of paramagnetic solids, the external magnetic field is used here only to align the magnetization of a sample along a certain direction.

The CPA formalism directly gives access to the configurationally averaged Green's function of disordered alloys. However, when calculating response functions for disordered alloys – as for example the conductivity given in in Eq. (98) – one has to deal with the configurational average of the product of two Green's functions. Within the framework of the KKR-formalism, this problem has first been investigated by Staunton [199] based on the work of Durham et al. [216]. With respect to the conductivity tensor a corresponding expression that is consistent with the single-site CPA-formalism has been worked out in great detail by Butler [212]. This approach, derived originally for the non-relativistic case, can straightforwardly be applied also for the spin polarized relativistic case [44] leading – in contrast to a non-relativistic scheme – in particular to an anisotropic conductivity tensor (see for example Eq. (99)). This makes clear that the galvano-magnetic effects AHR and SMA are all spin-orbit induced phenomena.

As an example of an application of the formalism sketched here the calculated isotropic resistivities $\bar{\rho}$ for the alloy systems $\text{Co}_x\text{Pd}_{1-x}$ and $\text{Co}_x\text{Pt}_{1-x}$ are shown in the left part of Fig. 10 [160] together with corresponding experimental data

measured at low temperature. As one can see, the agreement between calculated and measured resistivities is very good for Co_xPd_{1-x}. The maximum value of the resistivity in this system ($16\mu\Omega$·cm) as well as the composition for which the maximum occurs (about 20% Co) are well reproduced by the calculations.

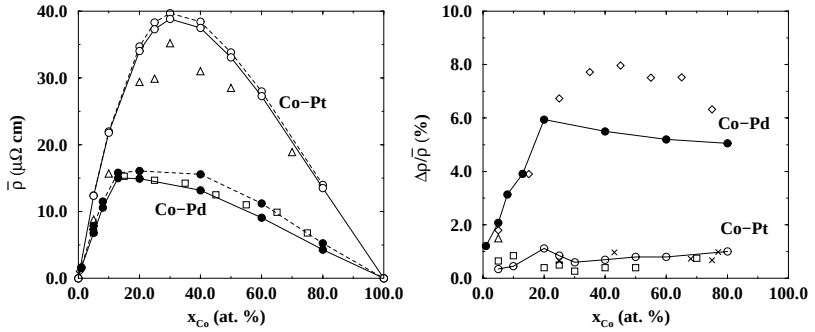

Fig. 10. Left: residual isotropic resistivity $\bar{\rho}$ of disordered Co_xPd_{1-x} (•) and Co_xPt_{1-x} (○) alloys. Full lines: calculated including vertex corrections, broken lines: calculated omitting vertex corrections. Right: calculated spontaneous magnetoresistance anisotropy (SMA) ratio $\Delta\rho/\bar{\rho}$ of Co_xPd_{1-x} (•) and Co_xPt_{1-x} (○) alloys. Experimental data presented by open squares, diamonds, triangles and crosses stem from various sources (see Ref. [160])

Using Butler's approach in dealing with Eq. (98) one accounts for the so-called vertex corrections within the framework of the CPA. For Co_xPd_{1-x} it was found that their contribution increases from about 2% for 5 at.% Co to about 25% for 80 at.% Co.

For the system Co_xPt_{1-x} the calculated resistivities are much higher than for Co_xPd_{1-x}, reaching almost 40 $\mu\Omega$·cm for 30 at% Co. This agrees in a satisfactory way with the experimental maximum of about 35 $\mu\Omega$·cm at that composition. In contrast to Co_xPd_{1-x} the vertex corrections are quite small for Co_xPt_{1-x}, contributing less than 3% to the total conductivity over the entire composition range. Previous investigations on paramagnetic alloy systems [217], lead to the conclusion that the vertex corrections are the more important the lower the d-like DOS at the Fermi level is. For Cu_xPt_{1-x} [217], for example, this applies to the noble metal rich side of this system. For ferromagnetic systems, on the other hand, the vertex corrections seem to be more important, if the d-like DOS at the Fermi level is low at least for one spin subsystem. For this reason, they are more pronounced for Co_xPd_{1-x} compared to Co_xPt_{1-x} and more important on the Co-rich side of both systems.

The anisotropy ratios (SMA) calculated from the transverse and longitudinal resistivities are shown in the right part of Fig. 10 for the two alloy systems Co_xPd_{1-x} and Co_xPt_{1-x}. Experimental values for both systems are included for comparison. Co_xPd_{1-x} shows remarkably high SMA values of more than 6%

for concentrations higher than 20 at.% Co [218,219]. The calculations reproduce the increase of the experimental data at low Co concentrations very well. For higher Co concentrations the calculated values are slightly too low. Note that the SMA in Co_xPd_{1-x} is still as large as 1.5% even for very low Co contents [219,220] which was attributed to local orbital moments on the magnetic sites in Ref. [219]. In contrast to Co_xPd_{1-x} the SMA for Co_xPt_{1-x} was found to be below 1% throughout the whole concentration range [221,222]. These findings are perfectly reproduced by the relativistic calculation which reflects the slowly varying SMA in Co_xPt_{1-x}.

It was realized already years ago that the SMA and also the AHR are caused by the spin-orbit coupling. Nevertheless, for the discussion of experimental data corresponding phenomenological descriptions had to be used in the past. These approaches were based on Mott's two-current model that ascribe to each spin subsystem an independent current contribution and introduced a number of model parameters. The SPR-KKR-CPA formalism, on the other hand, does not rely on Mott's two-current model and allows for a parameter-free and quantitative investigation of galvano-magnetic properties. By manipulating the strength of the spin-orbit coupling it was possible in particular to demonstrate explicitly the dependency of the SMA and the AHR on the spin-orbit coupling [223]. In addition it could be shown that even the isotropic resistivity $\bar{\rho}$ can be strongly influenced by the spin-orbit coupling, as it has been expected before [159].

Further insight into mechanisms giving rise to galvano-magnetic effects can be obtained by decomposition of the spin-orbit coupling. To demonstrate this, corresponding results for $\bar{\rho}$ and SMA ratio $\Delta\rho/\bar{\rho}$ are given in Fig. 11. The left

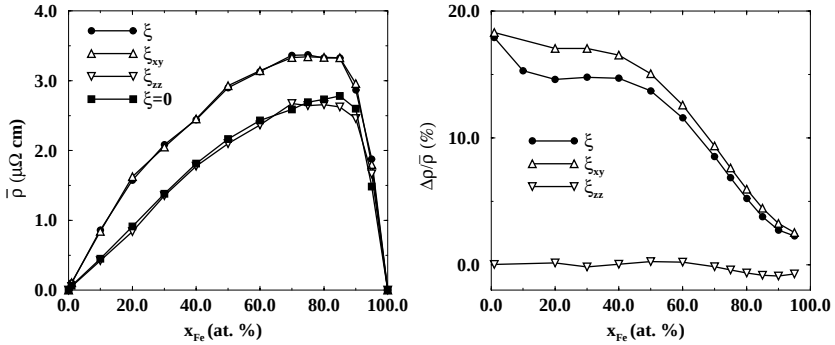

Fig. 11. Isotropic residual resistivity $\bar{\rho}$ (left), and spontaneous magnetoresistance anisotropy ratio $\Delta\rho/\bar{\rho}$ (right) of disordered bcc-Fe_xCo_{1-x} alloys calculated in four different ways. The results obtained using the full spin-orbit coupling – indicated by ξ – are represented by full circles. Open triangles give the results obtained keeping the xy-part ξ_{xy} and zz-part ξ_{zz}, respectively, of the spin-orbit coupling. Full squares give the result with the spin-orbit coupling completely suppressed ($\xi = 0$).

part of this figure shows the isotropic residual resistivity $\bar{\rho}$ of bcc-Fe_xCo_{1-x} ob-

tained from calculations using the full spin-orbit coupling (ξ). As one notes, the variation of $\bar{\rho}$ with composition is strongly asymmetric. This corresponds to the experimental findings [224,225]. The deviation from a parabolic shape can be qualitatively explained by the change of the DOS at the Fermi energy $n(E_{\rm F})$ that decreases monotonously with increasing Fe content. Keeping only the spin mixing part $\xi_{\rm xy}$ of the spin-orbit coupling (see Eq. (66)), one finds that $\bar{\rho}$ hardly changes. This already indicates that the spin mixing is the primary source for the relativistic enhancement of $\bar{\rho}$. This spin mixing or hybridization has already be demonstrated by means of the spin-projected Bloch spectral function $A_{\rm B}(\boldsymbol{k}, E)$ in Fig. 2 showing for fcc-$Fe_{0.2}Ni_{0.8}$ that there is an appreciable minority spin character admixed to the majority spin states which form a Γ-centered sheet of the Fermi surface and which primarily carry the electronic current [159,157]. Admixture of minority spin character clearly opens for these states a new scattering channel that is very effective because of the high DOS $n^{\downarrow}(E_{\rm F})$ at the Fermi energy with minority spin character. As a consequence, the total resistivity has to go up remarkably compared to a calculation based on the two-current model [161]. This interpretation is confirmed by the results obtained by keeping just $\xi_{\rm zz}$; i.e. suppressing the spin mixing effect of the spin-orbit coupling. In Fig. 11 one can see that this manipulation leads to a strong reduction of the total resistivity throughout the whole range of concentration. To demonstrate that the remaining part $\xi_{\rm zz}$ of the spin-orbit coupling has practically no influence on $\bar{\rho}$, an additional calculation has been carried out with the spin-orbit coupling completely suppressed ($\xi = 0$). The corresponding results nearly completely coincide with the $\xi_{\rm zz}$-data confirming this expectation. Here one should note that the latter calculational mode ($\xi = 0$) – although technically somewhat different – corresponds essentially to a calculation on the basis of the two-current model, where the electronic structure is calculated in a scalar relativistic way; i.e. with the relativistic corrections Darwin- and mass-velocity-terms taken into account [223].

For the spin-orbit induced SMA ratio the results obtained by the various calculations are given in the right part of Fig. 11. Here one finds that keeping only $\xi_{\rm xy}$ slightly reduces $\Delta\rho/\bar{\rho}$. This means that in contrast to $\bar{\rho}$, $\xi_{\rm zz}$ has some small effect on this quantity. Nevertheless, one finds that keeping $\xi_{\rm zz}$ alone brings $\Delta\rho/\bar{\rho}$ essentially to zero. From this result it can be concluded that the part $\xi_{\rm zz}$ of the spin-orbit coupling can in general be neglected as a source for the SMA compared to $\xi_{\rm xy}$. Finally, setting $\xi = 0$ of course reduces $\Delta\rho/\bar{\rho}$ exactly to zero [223].

The model calculations performed for the residual resistivity tensor elements of Fe_xCo_{1-x} allow to check the above mentioned phenomenological models for the galvano-magnetic effects. For example, Smit ascribed the occurrence of the SMA to the spin hybridization caused by the spin-orbit coupling [226]. From an analysis of experimental data, on the basis of corresponding expressions for $\Delta\rho/\bar{\rho}$, Jaoul et al. concluded that there should be an additional contribution due to the spin-diagonal part of the spin-orbit coupling [227]. The results presented in Fig. 11 clearly demonstrate that the mechanism discussed by Jaoul et al. can

be neglected for the isotropic resistivity $\bar{\rho}$ and has only minor contribution to the SMA in the case of the alloy system bcc-Fe_xCo_{1-x}.

Finally, it should mentioned that the expression for the conductivity tensor σ given in Eq. (98) has been generalized recently by Butler et al. [228] to deal with the giant magnetoresistance (GMR) of multilayer systems. A corresponding spin polarized relativistic formulation has been given by Weinberger et al. [229] that includes in particular the influence of the spin-orbit coupling. An extension of Eq. (98) to finite frequencies ω is also straightforward leading to absorptive part of the optical conductivity tensor $\sigma(\omega)$. This has been done recently by Banhart for the visible regime of the light and for paramagnetic alloy systems [230]. For ferromagnetic systems this extension gives directly access to the spin-orbit induced magneto-optical Kerr effect (MOKE) that has been investigated so far exclusively by means of conventional $\boldsymbol{k}$-space band structure methods as for example the SPR-LMTO [42]. The only exception to this is the work Huhne et al. [231], who developed a very general expression for $\sigma(\omega)$ within the framework of SPR-KKR. This approach should in particular supply a sound basis for an investigation of the oscillations of the Kerr-rotation observed for layered surface systems like Au/Fe/Au [232–234].

3.5 Spectroscopy

Magnetic Circular Dichroism in X-ray Absorption Magneto-optical effects in the visible regime of light are known now for more than 100 years [41,235] and it was realized more than 60 years ago that spin-orbit coupling plays a central role for these [236]. Guided by their experience with the magneto-optical Kerr effect (MOKE) Erskine and Stern [237] suggested that there should be a corresponding magnetic dichroism in X-ray absorption when circularly polarized radiation is used. This magnetic circular X-ray dichroism (MCXD) could be demonstrated for the first time for transition metals by Schütz et al. [43] by measurements at the K-edge of Fe in bcc-Fe in the XANES-region. Later on these authors could also observe the magnetic dichroism in the EXAFS region by investigation on the $L_{2,3}$-edge spectra of Gd in hcp-Gd [238]. Motivated by the MCXD-measurements on bcc-Fe a corresponding fully relativistic description has been developed that is based on the SPR-KKR-formalism [84,85] and that has been applied since then to a great variety of different systems [42]. Recently, this approach was extended to deal with magnetic EXAFS (MEXAFS) by making use of the cluster approximation for the multiple scattering representation of the final states.

Using the SPR-KKR-formalism the X-ray absorption coefficient $\mu^{\boldsymbol{q}\lambda}(\omega)$ is given by [42]:

$$\mu^{\boldsymbol{q}\lambda}(\omega) \propto \Im \sum_{i\,\mathrm{occ}} \left[\sum_{\Lambda\Lambda'} M_{\Lambda i}^{\boldsymbol{q}\lambda *}(E_i+\hbar\omega)\tau_{\Lambda\Lambda'}^{nm}(E_i+\hbar\omega)M_{\Lambda' i}^{\boldsymbol{q}\lambda}(E_i+\hbar\omega) + \sum_{\Lambda} I_{\Lambda i}^{\boldsymbol{q}\lambda}(E_i+\hbar\omega) \right] . \tag{101}$$

Here the sum i runs over all involved core states with energy E_i and wave function Φ_i. The electron-photon interaction operator $X_{\boldsymbol{q}\lambda}$, occurring in the matrix elements $M_{\Lambda i}^{\boldsymbol{q}\lambda}$, carries in particular information on the wave vector $\boldsymbol{q}$ of the radiation and on its polarization λ. The last term $I_{\Lambda i}^{\boldsymbol{q}\lambda}$ in Eq. (101) is an atomic-like matrix element [42] and is connected to the term in the Green's function involving the irregular solution to the Dirac equation (see Eq. (71)). Accordingly, it contributes only when working with complex energies.

Although there are also various forms of linear magnetic dichroism, most experimental investigations on the magnetic dichroism in X-ray absorption spectroscopy use circularly polarized radiation because the circular dichroism is most pronounced. To allow for a sound interpretation of the corresponding dichroic signal $\Delta\mu = \mu^+ - \mu^-$, given by the difference in absorption of left and right circularly polarized radiation, a set of so-called sum rules have been derived by several authors [239–242]. The main virtue of these rules is that they should allow one to obtain a reasonable estimate for expectation values $\langle\sigma_{\rm z}\rangle$ and $\langle l_{\rm z}\rangle$ of an absorber atom from its energy integrated dichroic signals $\int \Delta\mu(E)dE$. Of course, this is a very appealing property because these quantities are directly proportional to the spin and orbital magnetic moments, $\mu_{\rm spin}$ and $\mu_{\rm orb}$, respectively. However, in applying the sum rules one of the main problems is to fix the upper energy integration limit. For that reason it has been suggested to apply the sum rules in their differential form and to discuss the dichroic spectra $\Delta\mu(E)$ directly. For the $L_{2,3}$-edges these differential sum rules are given by [77]:

$$3\left[\Delta\mu_{\rm L_3} - 2\Delta\mu_{\rm L_2}\right] = C_{\rm d}\left(\frac{d}{dE}\langle\sigma_{\rm z}\rangle_{\rm d} + 7\frac{d}{dE}\langle T_{\rm z}\rangle_{\rm d}\right) \tag{102}$$

$$2\left[\Delta\mu_{\rm L_3} + \Delta\mu_{\rm L_2}\right] = C_{\rm d}\frac{d}{dE}\langle l_{\rm z}\rangle_{\rm d}\,. \tag{103}$$

Here $C_{\rm d}$ is a normalization constant and $T_{\rm z}$ is the magnetic dipole operator, that often can be ignored. Thus, the basic information to be deduced from the dichroic signal are the spin- and orbital polarization, $\frac{d}{dE}\langle\sigma_{\rm z}\rangle_{\rm d}$ and $\frac{d}{dE}\langle l_z\rangle_{\rm d}$, respectively, of final states with d-character.

The magnetic dichroism of the $L_{2,3}$-edge spectra of Pt in disordered Fe_xPt_{1-x} alloys has been studied experimentally as well as theoretically in great detail in the past [243–247]. Typically for Pt $L_{2,3}$-spectra it was found that the white lines at the L_2- and L_3-edges are quite different because of the influence of the spin-orbit coupling acting on the final states. This finding makes clear that a fully relativistic approach is indispensable to achieve a quantitative description of the $L_{2,3}$-absorption spectra of Pt. This applies in particular if one is dealing with magnetic EXAFS (MEXAFS). To deal with the MCXD in the X-ray absorption of Pt in ordered Fe_3Pt the scattering path operator $\tau_{\Lambda\Lambda'}^{nn}$ entering the expression for the absorption coefficient $\mu^{\boldsymbol{q}\lambda}$ was calculated using the matrix inversion technique for a cluster of 135 atoms in the XANES and 55 atoms in the EXAFS region, respectively, including the central absorber site. The effects of self-energy corrections [141,248] have been accounted for after calculating the spectra.

The top panel of Fig. 12 shows the results of calculations for the L_2-edge EXAFS-spectra of Pt in ordered Fe_3Pt. Corresponding experimental data, obtained by Ahlers and coworkers [249] for an ordered but slightly off-stoichiometric sample, are added. As one can see, the agreement of the theoretical and experimental spectra is quite satisfying, demonstrating in particular that the experimental sample is indeed ordered [250].

The circular dichroic spectrum $\Delta\mu_{L_2}$ for the L_2-edge is shown in the bottom panel of Fig. 12. Again a very satisfying agreement with the corresponding experimental results could be achieved. The results for $\Delta\mu_{L_2}$ clearly demonstrate that the occurrence of magnetic dichroism is by no means restricted to the white line region. Although the amplitude for $\Delta\mu_{L_2}$ is quite small compared to the white line region, it is present throughout the whole EXAFS-range.

As mentioned above, the applicability of the sum rules in their conventional form seems to be somewhat doubtful because of these findings. Nevertheless a clear-cut interpretation of the MEXAFS-spectra can be given making use of the sum rules in their differential form. In the upper part of Fig. 13 a superposi-

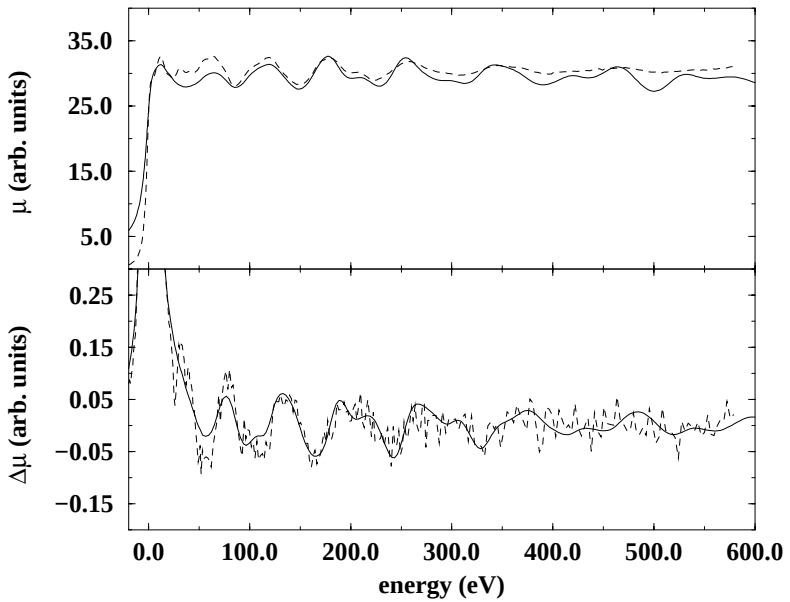

Fig. 12. EXAFS- (top) and MEXAFS-spectra (bottom) at the L_2-edge of Pt in Fe_3Pt. Calculations for the ordered compound (full line), compared against the experimental data for the $Fe_{0.72}Pt_{0.28}$ (dotted line) [249].

tion of the theoretical magnetic dichroism spectra $\Delta\mu_{L_2}$ and $\Delta\mu_{L_3}$ according to Eq. (102) is given (here the very small contribution $\frac{d}{dE}\langle T_z\rangle_d$ has been neglected). This is compared to the spin polarization $\frac{d}{dE}\langle\sigma_z\rangle_d$ of the d-states that have been

obtained directly from the band structure calculations. In the lower part of Fig. 13 the superposition according to Eq. (103) of the dichroic spectra is compared with the directly calculated orbital polarization $\frac{d}{dE}\langle l_{\rm z}\rangle_{\rm d}$ of the d-states. To compare the spectroscopic data with the band structure results the normalization factor $C_{\rm d}$ in Eq. (102) and (103) has been used as a free scaling parameter using the same value for the upper and lower part of Fig. 13.

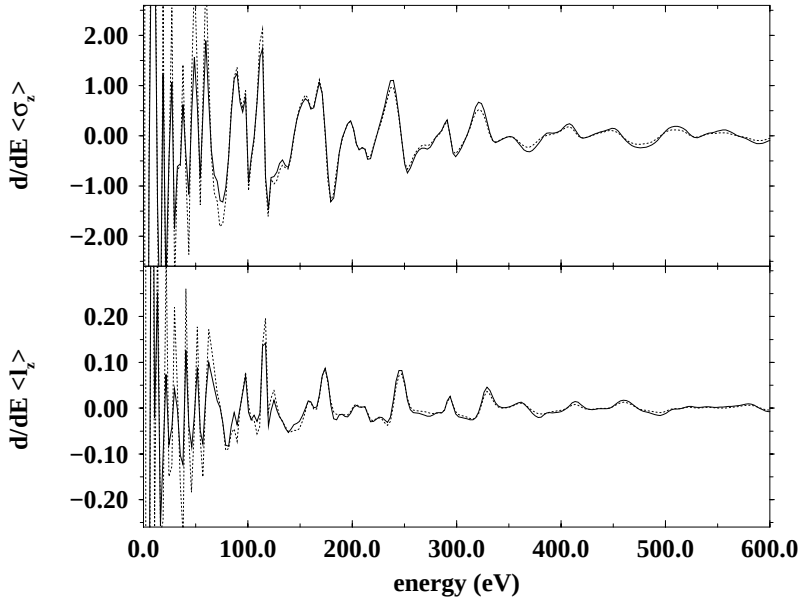

Fig. 13. Top: Spin polarization $\frac{d}{dE}\langle\sigma_{\rm z}\rangle_{\rm d}$ for the d-states of Pt (full line) compared to those derived from the MCXD-spectra using Eq. (102) (dashed line). Bottom: Orbital polarization $\frac{d}{dE}\langle l_{\rm z}\rangle_{\rm d}$ for the d-states of Pt (full line) compared to those derived from the MCXD-spectra using Eq. (103) (dashed line).

The nearly perfect coincidence of the various curves in the upper and lower part of Fig. 13 convincingly demonstrates that the primary information that can be deduced from circular $L_{2,3}$-MEXAFS spectra is the spin and orbital polarization for the final d-like states of the absorber atom. Of course, these are no pure atomic-like properties but concerning their variation with energy they strongly depend on the bonding to their surrounding. For this reason it is quite reasonable to perform a Fourier transform to the MEXAFS-spectra to seek for information on the magnetization distribution around the absorber atom [249]. However, the relationship of the magnetic radial distribution is by no means trivial. Nevertheless, it seems to be worth to investigate this relationship in more detail to be able to deduce further magnetic information from MEXAFS-spectra in a sound and reliable way.

Magnetic Dichroism in the VB-XPS Nowadays, the standard approach to deal with angular-resolved photoemission is to use the one-step model [251] together with the layer-KKR formalism [148]. A corresponding relativistic version for paramagnetic solids of this approach has been developed by Ackermann and Feder [252] and Ginatempo et al. [253] to study spin-orbit induced polarization effects in photoemission. In addition, a spin polarized relativistic and full-potential version has been introduced recently by Feder et al. [90] and Fluchtmann et al. [149] to deal with magnetic dichroic effects in magnetic solids. As an alternative to the above mentioned layer-KKR formalism, one can use the real-space multiple scattering formalism as well [254]. A corresponding expression for the time-reversed LEED-state used to represent the final states of a photo-emission experiment has been worked out first by Durham [255]. For the spin polarized relativistic case the LEED-state $\phi^{\mathrm{LEED}}_{\boldsymbol{k},m_s}(\boldsymbol{r},E)$ is given by [256]:

$$\phi^{\mathrm{LEED}}_{\boldsymbol{k},m_s}(\boldsymbol{r}_n,E) = 4\pi\sqrt{\frac{E+c^2}{2E+c^2}}\sum_{\Lambda} i^l\, C^{m_s}_{\Lambda}\, {Y_l^{\mu-m_s}}^*(\hat{\boldsymbol{k}}) \sum_m e^{i\boldsymbol{k}\boldsymbol{R}_m} \sum_{\Lambda'} \tau^{mn}_{\Lambda\Lambda'}(E)\, Z^n_{\Lambda'}(\boldsymbol{r}_n,E)\ . \tag{104}$$

where $\boldsymbol{k}$ and m_s denote the wave vector and spin character of the photo-electron. With the LEED-state available, it is straightforward to derive expressions for the photo-electron current intensity $I(E,m_s;\omega,\boldsymbol{q},\lambda)$ for any kind of photoemission experiment making use of Fermi's golden rule [251,256]. For excitation with high energy photons, multiple scattering may be neglected for the final states, leading to the so-called single scatterer approximation [257]. Dealing in addition with angle-integrated spectra leads to a rather simple expression for the photo-current intensity. In the case of VB-XPS one finds in particular [89]:

$$\begin{aligned} I(E,m_s;\omega,\boldsymbol{q},\lambda) \propto \sum_{\alpha} x_\alpha \Im \sum_{\substack{\Lambda\,\Lambda'' \\ \mu=\mu''}} C^{-m_s}_{\Lambda} C^{-m_s}_{\Lambda''} \\ \left\{ \sum_{\Lambda_1\,\Lambda_2} \tau^{0\,0,\,\alpha}_{\Lambda_1\Lambda_2}(E) \left[\sum_{\Lambda'} t^{0,\,\alpha}_{\Lambda'\Lambda}(E') M^{\boldsymbol{q}\lambda,\,\alpha}_{\Lambda'\Lambda_1}\right] \left[\sum_{\Lambda'''} t^{0,\,\alpha}_{\Lambda'''\Lambda''}(E') M^{\boldsymbol{q}\lambda,\,\alpha}_{\Lambda'''\Lambda_2}\right]^* \right. \\ \left. - \sum_{\Lambda'\,\Lambda'''\,\Lambda_1} t^{0,\,\alpha}_{\Lambda'\Lambda}(E') I^{\boldsymbol{q}\lambda,\,\alpha}_{\Lambda'\Lambda_1\Lambda'''} t^{0,\,\alpha *}_{\Lambda'''\Lambda''}(E') \right\}\ . \end{aligned} \tag{105}$$

Dealing with a paramagnetic solid this expression can be further simplified leading to the familiar result that the VB-XPS intensity is given by the sum over the κ- or angular-momentum j resolved DOS n_κ of the occupied part of the valence band with each contribution weighted by an appropriate cross-section σ_κ [258].

The spin polarized relativistic approach presented above has been applied among others to calculate the VB-XPS spectra of the disordered alloy system

Co_xPt_{1-x} [89]. Theoretical spectra for various concentrations are given in Fig. 14 for unpolarized radiation with $\hbar\omega = 1253.6$ eV. As can be seen, these spectra agree very well with corresponding experimental data reported by Weller and Reim [259].

As mentioned above, for the paramagnetic case the expression for the photo current in Eq. (105) can be simplified to a concentration weighted sum over the products of the κ-resolved partial DOS $n^{\kappa}_{\alpha}(E)$ and a corresponding matrix element that smoothly varies with energy [258]. This means that the XPS-spectra map the DOS-curves in a rather direct way. This essentially holds also for the spin-polarized case. As can be seen from the DOS curves of Co_xPt_{1-x} (see for example Ref. [89]) both components retain the gross features of their electronic structure when they are combined to an alloy system: while Co has a narrow and strongly exchange-split d-band complex close to the Fermi level, the Pt d-band is rather broad and only slightly spin-split due to hybridization in the region of the Co d-band. This behavior supplies a very simple explanation for the variation of the spectra in Fig. 14 with composition and allows one to ascribe prominent features as shoulders and peaks to either Co or Pt. Nevertheless, one has to note that these spectra are not just a concentration weighted sum of the spectra for pure Co and pure Pt. One reason for this is that there are non-negligible changes of the component-resolved DOS-curves compared to those of the pure constituents. In addition one can see from Fig. 14 that for the selected photon energy the partial photoemission absorption cross section that depends on the initial state energy E as well as the photon energy $\hbar\omega$ is about a factor of two higher for Pt than for Co.

Performing angular-resolved photoemission experiments for disordered alloys seems to be profitable only in some favorable cases for which disorder does not prevent the existence of a rather well-defined dispersion relation [260]. While this applies for example to Fe_xNi_{1-x} (see Fig. 2) this is surely not the case

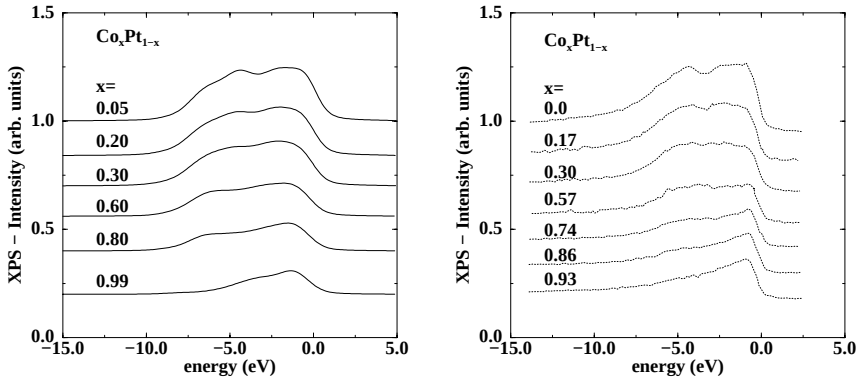

Fig. 14. Theoretical VB-XPS spectra (left) for Co_xPt_{1-x} for unpolarized radiation and photon energy $\hbar\omega = 1253.6$ eV. The corresponding experimental data (right) have been taken from Weller and Reim [259].

for Co_xPt_{1-x}. Nevertheless, deeper insight into its electronic structure and in particular its magnetic aspects can be obtained by VB-XPS experiments done using circularly polarized radiation. In the case of Co_xPt_{1-x} [89] but also for Fe_xCo_{1-x} [261] the calculation of the VB-XPS spectra predict a non-negligible circular dichroism even for the angular averaged spectra that should be strong enough to be detected within an experiment (corresponding measurements have not yet been done). The circular dichroism occurs primarily in the region of pronounced spin-polarization and has the same sign throughout that energy region. This behavior differs from that of the angular resolved theoretical spectra obtained by Scheunemann et al. [90] for the normal emission from perpendicular magnetized Ni (001) that show a circular dichroism that change sign with binding energy with the energy integrated dichroism spectrum essentially vanishing [90]. While these specific spectra map states well below the Fermi energy with both spin characters contributing roughly to the same extent, the angular integrated spectra are dominated by the majority spin character [89]. Therefore, shifting the Fermi energy artificially to higher energies should result in a reversal in sign for the dichroism in the VB-XPS spectrum with the energy integrated signal going to zero.

A more pronounced circular dichroism than for the spin-averaged case is found for the spin-polarized case, with corresponding spectra given in Fig. 15. Again the circular dichroism occurs primarily in the energy region showing pro-

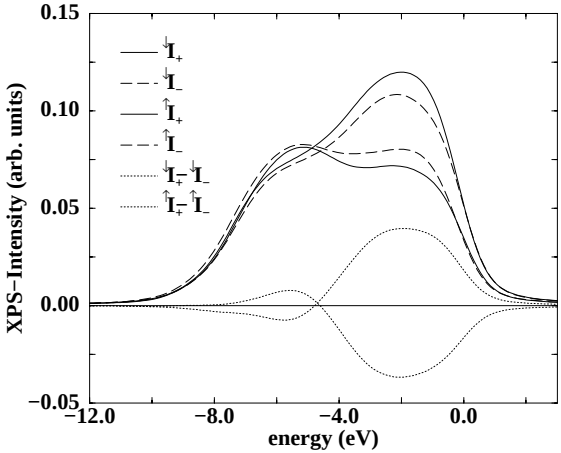

Fig. 15. Theoretical spin-resolved VB-XPS spectra of $Co_{0.6}Pt_{0.4}$ for circularly polarized radiation and photon energy $\hbar\omega = 1253.6$ eV.

nounced spin-polarization. Comparing the circular dichroism signal for the two different spin characters one notes that they are opposite in sign. This behavior has also been found before for the spin-resolved spectra mentioned above and

explained as a direct consequence of the spin orbit coupling [90]. Finally it should be mentioned that circular dichroism spectra similar to that shown in Fig. 15 are found if the photon energy $\hbar\omega$ is varied. Setting $\hbar\omega$ to a value for which one of the components possess a Cooper minimum allows one to get additional component specific information. This could supply very helpful information on the nature of the initial states and the contribution of the various components for the very complex magneto-optical Kerr-rotation spectra of transition metal alloys and compounds [262].

4 Summary

The formal background to deal with the electronic structure of magnetic solids, accounting simultaneously for relativistic effects, has been reviewed. The main emphasize has been laid on a four-component formalism that is based on a Dirac equation set up within the framework of DFT. As recent developments in this field, the inclusion of the Breit-interaction and the use of CDFT has been discussed. Solving the corresponding single site problem allows in principle to set up for any band structure method the necessary four-component spherical basis functions that account on a corresponding level of sophistication simultaneously and on the same footing for magnetic order and relativity. Here, the KKR-method has been used and accordingly several recent developments concerning this – as the incorporation of the OP-formalism, the full-potential formalism or the TB-version – have been discussed or mentioned. The main motivation for using the KKR-method stems from the fact that all features of the underlying Hamiltonian are directly incorporated in the corresponding wave functions, in contrast to schemes that account for corrections to an unperturbed Hamiltonian within a variational procedure. In addition, it directly gives access to the electronic Green's function. This very appealing feature has been exploited within many of the presented applications, as for example in the case of impurity systems lacking Bloch-symmetry.

Independent of the use of the KKR-method, the presented applications demonstrated that the spin-orbit coupling influences the properties of magnetic solids in various, quite different, ways. In some cases one gets just a correction to results that are obtained by a non- or scalar relativistic calculation. Of course, most interesting are pure spin-orbit induced properties that would not occur if the spin-orbit coupling or magnetic order would be absent. Nearly all properties discussed here fall into this category.

Using the full Dirac-formalism to deal with magnetic systems is of course very satisfying from a formal point of view but makes it in general quite cumbersome to give a simple interpretation of the numerical results. For this reason, approximate schemes, as those presented here, are very helpful and important for the discussion of the various spin-orbit induced properties. In particular, they allow to decide which consequence of the spin-orbit coupling is more important: lifting of energetic degeneracies or spin-hybridization. Concerning this question,

it was demonstrated that the relevance of this two effects can be quite different for a spin-orbit induced property.

Altogether, one can claim that in general a rather satisfying quantitative agreement of theoretical and experimental data can be achieved when calculating spin-orbit induced properties. Remarkable deviations occur primarily if one is investigating properties closely connected with orbital magnetism. The most promising way to remove these problems in a consistent way, i.e. in particular within the framework of DFT, is to apply CDFT. Because of the delicate situation it might be necessary to perform the corresponding calculations in the full-potential mode and/or to use the optimized effective potential (OEP) scheme in addition. Anyhow, whatever will happen in this and related fields in the future, working with the four-component Dirac-Green's function-formalism will guaranty that one is open and prepared for any new developments.

Acknowledgment

The author would like to thank H. Akai, D. Ahlers, J. Banhart, M. Battocletti, P. H. Dederichs, M. Deng, H. Freyer, E. K. U. Gross, B. L. Gyorffy, T. Huhne, V. Popescu, J. Schwitalla, P. Strange, W. Temmerman, C. Zecha, R. Zeller, and A. Vernes for their fruitful and pleasant collaboration during the last years. The common work presented here benefited a lot from financial support and collaborations within the HCM-networks *Ab-initio (from electronic structure) calculation of complex processes in materials* and *Novel probes for magnetic materials and magnetic phenomena: linear and circular X-ray dichroism*, the TMR-network on *Ab-initio Calculations of Magnetic Properties of Surfaces, Interfaces and Multilayers* of the European Union, the programme *Relativistic Effects in Heavy-Element Chemistry and Physics (REHE)* of the European Science Foundation, the programme *Theorie relativistischer Effekte in der Chemie und Physik schwerer Elemente* funded by the DFG (Deutsche Forschungsgemeinschaft) and the programme *Zirkular polarisierte Synchrotronstrahlung: Dichroismus, Magnetismus und Spinorientierung* run by the German ministry for research and technology (BMBF).

References

1. N. E. Christensen and B. O. Seraphin, Phys. Rev. B **4**, 3321 (1971).
2. P. Pyykkö, Adv. Quantum. Chem. **11**, 353 (1978).
3. Y. Cauchois and I. Manescu, C. R. Acad. Sci. **210**, 172 (1940).
4. N. F. Mott, Proc. Phys. Soc. A **62**, 416 (1949).
5. A. R. Mackintosh and O. K. Andersen, in *Electrons at the Fermi Surface*, edited by M. Springford (Cambridge University Press, Cambridge, 1980), Chap. The Electronic Structure of Transition Metals.
6. L. Tterlikkis, S. D. Mahanti, and T. P. Das, Phys. Rev. **176**, 10 (1968).
7. M. E. Rose, *Relativistic Electron Theory* (Wiley, New York, 1961).
8. F. Rosicky and F. Mark, J. Phys. B: Atom. Molec. Phys. **8**, 2581 (1975).

9. F. Rosicky, P. Weinberger, and F. Mark, J. Phys. B: Atom. Molec. Phys. **9**, 2971 (1976).
10. D. D. Koelling and B. N. Harmon, J. Phys. C: Solid State Phys. **10**, 3107 (1977).
11. H. Gollisch and L. Fritsche, phys. stat. sol. (b) **86**, 145 (1978).
12. T. Takeda, Z. Physik B **32**, 43 (1978).
13. J. H. Wood and A. M. Boring, Phys. Rev. B **18**, 2701 (1978).
14. H. L. Skriver, *The LMTO-method* (Springer, Berlin, 1983).
15. N. J. M. Geipel and B. A. Hess, Chem. Phys. Lett. **273**, 62 (1997).
16. E. van Lenthe E J Baerends and J. G. Snijders, J. Chem. Phys. **101**, 1272 (1994).
17. F. Gesztesy, H. Grosse, and B. Thaller, Ann. Inst. Poincaré **40**, 159 (1984).
18. C. Brouder, M. Alouani, and K. H. Bennemann, Phys. Rev. B **54**, 7334 (1996).
19. D. D. Koelling and A. H. MacDonald, in *Relativistic Effects in Atoms Molecules and Solids*, edited by G. L. Malli (Plenum Press, New York, 1983).
20. S. Blügel, H. Akai, R. Zeller, and P. H. Dederichs, Phys. Rev. B **35**, 3271 (1987).
21. T. Gasche, Ph.D. thesis, University of Uppsala, 1993.
22. J. E. Lee, C. L. Fu, and A. J. Freeman, J. Magn. Magn. Materials **62**, 93 (1986).
23. T. Asada and K. Terakura, J. Phys. F: Met. Phys. **12**, 1387 (1982).
24. H. Ebert, P. Strange, and B. L. Gyorffy, J. Phys. F: Met. Phys. **18**, L135 (1988).
25. H. Ebert and H. Akai, Hyperfine Interactions **78**, 361 (1993).
26. C. S. Wang and J. Callaway, Phys. Rev. B **9**, 4897 (1974).
27. D. K. Misemer, J. Magn. Magn. Materials **72**, 267 (1988).
28. G. Y. Guo and H. Ebert, Phys. Rev. B **51**, 12633 (1995).
29. J. Callaway and C. S. Wang, Phys. Rev. B **7**, 1096 (1973).
30. O. K. Andersen, Phys. Rev. B **12**, 3060 (1975).
31. D. Singh, *Plane Waves, Pseudopotentials and the LAPW Method* (Kluwer Academic, Amsterdam, 1994).
32. A. Delin, P. Ravindran, O. Eriksson, and J. M. Wills, Intern. J. Quantum. Chem. **69**, 349 (1997).
33. T. L. Loucks, Phys. Rev. A **139**, 1333 (1965).
34. P. Soven, Phys. Rev. **137**, A 1706 (1965).
35. Y. Onodera and M. Okazaki, J. Phys. Soc. Japan **21**, 1273 (1966).
36. S. Takada, Progr. Theor. Phys. Suppl. **36**, 224 (1966).
37. T. Takeda, J. Phys. F: Met. Phys. **9**, 815 (1979).
38. U. Fano, Phys. Rev. **184**, 250 (1969).
39. U. Fano, Phys. Rev. **178**, 131 (1969).
40. U. Heinzmann, K. Jost, J. Kessler, and B. Ohnemus, Z. Physik **251**, 354 (1972).
41. J. Kerr, Phil. Mag. **3**, 321 (1877).
42. H. Ebert, Rep. Prog. Phys. **59**, 1665 (1996).
43. G. Schütz *et al.*, Phys. Rev. Letters **58**, 737 (1987).
44. J. Banhart and H. Ebert, Europhys. Lett. **32**, 517 (1995).
45. B. Újfalussy, L. Szunyogh, P. Bruno, and P. Weinberger, Phys. Rev. Letters **77**, 1805 (1996).
46. G. Seewald *et al.*, Phys. Rev. Letters **78**, 1795 (1997).
47. M. Singh, C. S. Wang, and J. Callaway, Phys. Rev. B **11**, 287 (1975).
48. M. S. S. Brooks and P. J. Kelly, Phys. Rev. Letters **51**, 1708 (1983).
49. J. Sticht and J. Kübler, Solid State Commun. **53**, 529 (1985).
50. W. M. Temmerman and P. A. Sterne, J. Phys.: Condensed Matter **2**, 5529 (1990).
51. O. Eriksson *et al.*, Phys. Rev. B **42**, 2707 (1990).
52. S. P. Lim, D. L. Price, and B. R. Cooper, IEEE transactions on magnetics **27**, 3648 (1991).

53. B. I. Min and Y.-R. Jang, J. Phys.: Condensed Matter **3**, 5131 (1991).
54. O. Hjortstam *et al.*, Phys. Rev. B **53**, 9204 (1996).
55. D. S. Wang, R. Q. Wu, L. P. Z. LP, and A. J. Freeman, J. Magn. Magn. Materials **144**, 643 (1995).
56. V. P. Antropov, A. I. Liechtenstein, and B. N. Harmon, J. Magn. Magn. Materials **140-144**, 1161 (1995).
57. H. Ebert, Phys. Rev. B **38**, 9390 (1988).
58. J. M. MacLaren and R. H. Victora, J. Appl. Physics **76**, 6069 (1994).
59. H. Akai, private communication, 1995.
60. A. Ankudinov, Ph.D. thesis, University of Washington, 1985.
61. A. K. Rajagopal and J. Callaway, Phys. Rev. B **7**, 1912 (1973).
62. U. von Barth and L. Hedin, J. Phys. C: Solid State Phys. **5**, 1629 (1972).
63. A. H. MacDonald and S. H. Vosko, J. Phys. C: Solid State Phys. **12**, 2977 (1979).
64. M. V. Ramana and A. K. Rajagopal, Adv. Chem. Phys. **54**, 231 (1983).
65. M. Richter and H. Eschrig, Solid State Commun. **72**, 263 (1989).
66. S. Doniach and C. Sommers, in *Valence Fluctuations in Solids*, edited by L. M. Falicov, W. Hanke, and M. B. Maple (North-Holland, Amsterdam, 1981), p. 349.
67. R. Feder, F. Rosicky, and B. Ackermann, Z. Physik B **52**, 31 (1983).
68. P. Strange, J. B. Staunton, and B. L. Gyorffy, J. Phys. C: Solid State Phys. **17**, 3355 (1984).
69. I. V. Solovyev *et al.*, Soviet Physics - Solid State **31**, 1285 (1989).
70. B. C. H. Krutzen and F. Springelkamp, J. Phys.: Condensed Matter **1**, 8369 (1989).
71. B. Ackermann, R. Feder, and E. Tamura, J. Phys. F: Met. Phys. **14**, L173 (1984).
72. G. Schadler, R. C. Albers, A. M. Boring, and P. Weinberger, Phys. Rev. B **35**, 4324 (1987).
73. H. Ebert, B. Drittler, and H. Akai, J. Magn. Magn. Materials **104-107**, 733 (1992).
74. L. Szunyogh, B. Újfalussy, P. Weinberger, and J. Kollar, Phys. Rev. B **49**, 2721 (1994).
75. R. Zeller *et al.*, Phys. Rev. B **52**, 8807 (1995).
76. H. Ebert, V. Popescu, and D. Ahlers, J. Phys. (Paris) **7**, C2 131 (1997).
77. H. Ebert, V. Popescu, and D. Ahlers, Phys. Rev. B, submitted (1998).
78. S. V. Beiden *et al.*, Phys. Rev. B **57**, 14247 (1998).
79. E. Tamura, Phys. Rev. B **45**, 3271 (1992).
80. X. Wang *et al.*, Phys. Rev. B **46**, 9352 (1992).
81. S. C. Lovatt, B. L. Gyorffy, and G.-Y. Guo, J. Phys.: Condensed Matter **5**, 8005 (1993).
82. T. Huhne, Master's thesis, University of Munich, 1997.
83. T. Huhne *et al.*, Phys. Rev. B **58**, 10236 (1998).
84. H. Ebert, P. Strange, and B. L. Gyorffy, J. Appl. Physics **63**, 3055 (1988).
85. H. Ebert, P. Strange, and B. L. Gyorffy, Z. Physik B **73**, 77 (1988).
86. P. Strange, P. J. Durham, and B. L. Gyorffy, Phys. Rev. Letters **67**, 3590 (1991).
87. E. Tamura, G. D. Waddill, J. G. Tobin, and P. A. Sterne, Phys. Rev. Letters **73**, 1533 (1994).
88. H. Ebert, L. Baumgarten, C. M. Schneider, and J. Kirschner, Phys. Rev. B **44**, 4466 (1991).
89. H. Ebert and J. Schwitalla, Phys. Rev. B **55**, 3100 (1997).
90. T. Scheunemann, S. V. Halilov, J. Henk, and R. Feder, Solid State Commun. **91**, 487 (1994).

91. E. Arola, P. Strange, and B. L. Gyorffy, Phys. Rev. B **55**, 472 (1997).
92. H. J. Gotsis and P. Strange, J. Phys.: Condensed Matter **6**, 1409 (1994).
93. A. B. Shick, V. Drchal, J. Kudrnovský, and P. Weinberger, Phys. Rev. B **54**, 1610 (1996).
94. P. Weinberger, I. Turek, and L. Szunyogh, Intern. J. Quantum. Chem. **63**, 165 (1997).
95. I. Turek *et al.*, *Electronic structure of disordered alloys, surfaces and interfaces* (Kluwer Academic Publ., Boston, 1997).
96. R. M. Dreizler and E. K. U. Gross, *Density Functional Theory* (Springer-Verlag, Heidelberg, 1990).
97. H. Eschrig, *The Fundamentals of Density Functional Theory* (B G Teubner Verlagsgesellschaft, Stuttgart, Leipzig, 1996).
98. A. H. MacDonald, J. Phys. C: Solid State Phys. **16**, 3869 (1983).
99. A. K. Rajagopal, J. Phys. C: Solid State Phys. **11**, L943 (1978).
100. M. V. Ramana and A. K. Rajagopal, J. Phys. C: Solid State Phys. **12**, L845 (1979).
101. H. Eschrig, G. Seifert, and P. Ziesche, Solid State Commun. **56**, 777 (1985).
102. B. X. Xu, A. K. Rajagopal, and M. V. Ramana, J. Phys. C: Solid State Phys. **17**, 1339 (1984).
103. M. V. Ramana and A. K. Rajagopal, J. Phys. C: Solid State Phys. **14**, 4291 (1981).
104. G. Vignale and M. Rasolt, Phys. Rev. Letters **59**, 2360 (1987).
105. G. Vignale and M. Rasolt, Phys. Rev. B **37**, 10685 (1988).
106. G. Vignale and M. Rasolt, Phys. Rev. Letters **62**, 115 (1989).
107. G. Vignale, in *Current Density Functional Theory and Orbital Magnetism*, Vol. 337 of *Nato ASI Series, Series B*, edited by E. K. U. Gross and R. M. Dreizler (Plenum Press, NewYork, 1995), p. 485.
108. P. Skudlarski and G. Vignale, Phys. Rev. B **48**, 8547 (1993).
109. H. Ebert, M. Battocletti, and E. K. U. Gross, Europhys. Lett. **40**, 545 (1997).
110. H. Bethe and E. Salpeter, *Quantum Mechanics of One- and Two-Electron Atoms* (Springer, New York, 1957).
111. H. J. F. Jansen, J. Appl. Physics **64**, 5604 (1988).
112. H. Ebert, unpublished (1995).
113. M. S. S. Brooks, Physica B **130**, 6 (1985).
114. O. Eriksson, B. Johansson, and M. S. S. Brooks, J. Phys.: Condensed Matter **1**, 4005 (1989).
115. O. Eriksson, M. S. S. Brooks, and B. Johansson, Phys. Rev. B **41**, 7311 (1990).
116. L. Severin, M. S. S. Brooks, and B. Johansson, Phys. Rev. Letters **71**, 3214 (1993).
117. A. B. Shick and V. A. Gubanov, Phys. Rev. B **49**, 12860 (1994).
118. H. Ebert and M. Battocletti, Solid State Commun. **98**, 785 (1996).
119. G. Racah, Phys. Rev. **42**, 438 (1942).
120. R. Pittini, J. Schoenes, O. Vogt, and P. Wachter, Phys. Rev. Letters **77**, 944 (1996).
121. W. M. Temmerman, Z. Szotek, and G. A. Gehring, Phys. Rev. Letters **79**, 3970 (1997).
122. J. Forstreuter, L. Steinbeck, M. Richter, and H. Eschrig, Phys. Rev. B **55**, 9415 (1997).
123. E. Engel *et al.*, Phys. Rev. A **58**, 964 (1998).
124. A. H. MacDonald, J. M. Daams, S. H. Vosko, and D. D. Koelling, Phys. Rev. B **23**, 6377 (1981).

125. L. Severin, M. Richter, and L. Steinbeck, Phys. Rev. B **55**, 9211 (1997).
126. R. N. Schmid *et al.*, Adv. Quantum. Chem. in press (1999).
127. P. Cortona, S. Doniach, and C. Sommers, Phys. Rev. A **31**, 2842 (1985).
128. B. Ackermann, Ph.D. thesis, University of Duisburg, 1985.
129. A. C. Jenkins and P. Strange, J. Phys.: Condensed Matter **6**, 3499 (1994).
130. B. Drittler, H. Ebert, R. Zeller, and P. H. Dederichs, Phys. Rev. B **67**, 4573 (1990).
131. P. H. Dederichs, B. Drittler, and R. Zeller, Mat. Res. Soc. Symp. Proc. **253**, 185 (1992).
132. O. K. Andersen and R. G. Wooley, Molecular Physics **26**, 905 (1973).
133. J. S. Faulkner, J. Phys. C: Solid State Phys. **10**, 4661 (1977).
134. J. S. Faulkner, Phys. Rev. B **19**, 6186 (1979).
135. H. Ebert and B. L. Gyorffy, J. Phys. F: Met. Phys. **18**, 451 (1988).
136. J. S. Faulkner and G. M. Stocks, Phys. Rev. B **21**, 3222 (1980).
137. H. Ebert, H. Freyer, A. Vernes, and G.-Y. Guo, Phys. Rev. B **53**, 7721 (1996).
138. H. Ebert, H. Freyer, and M. Deng, Phys. Rev. B **56**, 9454 (1997).
139. H. Ebert, habilitaion thesis, University of München, 1990.
140. B. L. Gyorffy and M. J. Stott, in *Band Structure Spectroscopy of Metals and Alloys*, edited by D. J. Fabian and L. M. Watson (Academic Press, New York, 1973), p. 385.
141. T. Fujikawa, R. Yanagisawa, N. Yiwata, and K. Ohtani, J. Phys. Soc. Japan **66**, 257 (1997).
142. H. Wu and S. Y. Tong, Phys. Rev. B submitted (1998).
143. A. P. Cracknell, J. Phys. C: Solid State Phys. **2**, 1425 (1969).
144. A. P. Cracknell, Phys. Rev. B **1**, 1261 (1970).
145. G. Hörmandinger and P. Weinberger, J. Phys.: Condensed Matter **4**, 2185 (1992).
146. C. Zecha, Master's thesis, University of Munich, 1997.
147. C. Kornherr, Master's thesis, University of Munich, 1997.
148. J. B. Pendry, *Low energy electron diffraction* (Academic Press, London, 1974).
149. M. Fluchtmann, J. Braun, and G. Borstel, Phys. Rev. B **52**, 9564 (1995).
150. L. Szunyogh, B. Újfalussy, and P. Weinberger, Phys. Rev. B **51**, 9552 (1995).
151. R. Zeller, P. Lang, B. Drittler, and P. H. Dederichs, Mat. Res. Soc. Symp. Proc. **253**, 357 (1992).
152. T. Huhne, Ph.D. thesis, University of München, in preparation, 1989.
153. B. Nonas, Ph.D. thesis, RWTH Aachen, in preparation, 1989.
154. P. Soven, Phys. Rev. **156**, 809 (1967).
155. P. Strange, H. Ebert, J. B. Staunton, and B. L. Gyorffy, J. Phys.: Condensed Matter **1**, 2959 (1989).
156. J. S. Faulkner, Prog. Mater. Sci. **27**, 1 (1982).
157. H. Ebert, A. Vernes, and J. Banhart, Solid State Commun. **104**, 243 (1997).
158. H. Eckardt and L. Fritsche, J. Phys. F: Met. Phys. **17**, 925 (1987).
159. I. Mertig, R. Zeller, and P. H. Dederichs, Phys. Rev. B **47**, 16178 (1993).
160. H. Ebert, J. Banhart, and A. Vernes, Phys. Rev. B **54**, 8479 (1996).
161. J. Banhart, H. Ebert, and A. Vernes, Phys. Rev. B **56**, 10165 (1997).
162. A. B. Shick, D. L. Novikov, and A. J. Freeman, Phys. Rev. B **56**, R14259 (1997).
163. A. B. Shick, D. L. Novikov, and A. J. Freeman, J. Appl. Physics **83**, 7258 (1998).
164. X. Wang, D. Wang, R. Wu, and A. J. Freeman, J. Magn. Magn. Materials **159**, 337 (1996).
165. G. H. O. Daalderop, P. J. Kelly, and M. F. H. Schuurmans, Phys. Rev. B **41**, 11919 (1990).

166. P. Strange, J. B. Staunton, and H. Ebert, Europhys. Lett. **9**, 169 (1989).
167. Újfalussy, L. Szunyogh, and P. Weinberger, in *Properties of Complex Inorganic Solids*, edited by A. Gonis, A. Meike, and P. E. A. Turchi (Plenum Press, New York, 1997), p. 181.
168. V. A. Gubanov, A. I. Lichtenstejn, and A. V. Postnikov, *Magnetism and the electronic structure of crystals* (Springer, Berlin, 1992).
169. S. S. A. Razee, J. B. Staunton, and F. J. Pinski, Phys. Rev. B **56**, 8082 (1997).
170. G. Y. Guo, H. Ebert, and W. M. Temmerman, J. Phys.: Condensed Matter **3**, 8205 (1991).
171. G. Y. Guo, H. Ebert, and W. M. Temmerman, J. Magn. Magn. Materials **104-107**, 1772 (1992).
172. M. B. Stearns, in *Magnetic Properties of 3d, 4d and 5d Elements, Alloys and Compounds*, Vol. III/19a of *Landolt-Börnstein, New Series*, edited by K.-H. Hellwege and O. Madelung (Springer, Berlin, 1987).
173. O. Eriksson *et al.*, Phys. Rev. B **41**, 11807 (1990).
174. J. Trygg, B. Johansson, O. Eriksson, and J. M. Wills, Phys. Rev. Letters **75**, 2871 (1995).
175. P. Söderlind *et al.*, Phys. Rev. B **45**, 12911 (1992).
176. M. S. S. Brooks and B. Johansson, in *Spin-orbit influenced spectroscopies of magnetic solids*, Vol. 466 of *Lecture Notes in Physics*, edited by H. Ebert and G. Schütz (Springer, Berlin, 1996), p. 211.
177. G. H. O. Daalderop, P. J. Kelly, and M. F. H. Schuurmans, Phys. Rev. B **44**, 12054 (1991).
178. H. Ebert, A. Vernes, and J. Banhart, Phys. Rev. B submitted (1998).
179. Gasche, M. S. S. Brooks, and B. Johansson, Phys. Rev. B **53**, 296 (1996).
180. H. Ebert, Solid State Commun. **100**, 677 (1996).
181. P. Herzig, Theoret. Chim. Acta. (Berlin) **67**, 323 (1985).
182. M. Battocletti, Ph.D. thesis, University of München, 1997.
183. P. C. Riedi and E. Hagn, Phys. Rev. B **30**, 5680 (1984).
184. M. Aiga and J. Itoh, J. Phys. Soc. Japan **37**, 967 (1974).
185. Eder, E. Hagn, and E. Zech, Phys. Rev. C **32**, 582 (1985).
186. M. Kawakami, H. Enokiya, and T. Okamoto, J. Phys. F: Met. Phys. **15**, 1613 (1985).
187. P. Blaha, K. Schwarz, and P. H. Dederichs, Phys. Rev. B **37**, 2792 (1988).
188. H. Ebert, R. Zeller, B. Drittler, and P. H. Dederichs, J. Appl. Physics **67**, 4576 (1990).
189. G. A. Gehring and H. C. W. L. Williams, J. Phys. F: Met. Phys. **4**, 291 (1974).
190. C. Demangeat, J. Phys. F: Met. Phys. **5**, 169 (1975).
191. G. Y. Guo and H. Ebert, Phys. Rev. B **50**, 10377 (1994).
192. D. Weller *et al.*, Phys. Rev. Letters **72**, 2097 (1994).
193. G. Breit, Phys. Rev. **35**, 1447 (1930).
194. N. C. Pyper, Molecular Physics **64**, 933 (1988).
195. A. Abragam and M. H. L. Pryce, Proc. Roy. Soc. (London) A **205**, 135 (1951).
196. M. Battocletti, H. Ebert, and H. Akai, Phys. Rev. B **53**, 9776 (1996).
197. H. Akai and T. Kotani, Hyperfine Interactions, in press (1998).
198. K. Terakura, N. Hamada, T. Oguchi, and T. Asada, J. Phys. F: Met. Phys. **12**, 1661 (1982).
199. J. B. Staunton, Ph.D. thesis, University of Bristol, 1982.
200. M. Matsumoto, J. B. Staunton, and P. Strange, J. Phys.: Condensed Matter **2**, 8365 (1990).

201. M. Matsumoto, J. B. Staunton, and P. Strange, J. Phys.: Condensed Matter **3**, 1453 (1991).
202. J. F. Janak, Phys. Rev. B **16**, 255 (1977).
203. J. Benkowitsch and Winter, J. Phys. F: Met. Phys. **13**, 991 (1983).
204. J. Benkowitsch and Winter, Physica Scripta **31**, 222 (1985).
205. H. Ebert, Ph.D. thesis, University of München, 1986.
206. H. Ebert, H. Winter, and J. Voitländer, J. Phys. F: Met. Phys. **16**, 1133 (1986).
207. M. Yasui and M. Shimizu, J. Phys. F: Met. Phys. **9**, 1653 (1979).
208. M. Yasui and M. Shimizu, J. Phys. F: Met. Phys. **15**, 2365 (1985).
209. G. C. Carter, L. H. Bennett, and D. J. Kahan, Prog. Mater. Sci. **20**, 153 (1977).
210. I. V. Solovyev, P. H. Dederichs, and I. Mertig, Phys. Rev. B **5**, 13419 (1995).
211. D. A. Greenwood, Proc. Phys. Soc. **71**, 585 (1958).
212. W. H. Butler, Phys. Rev. B **31**, 3260 (1985).
213. W. H. Kleiner, Phys. Rev. **142**, 318 (1966).
214. P. R. Birss, *Selected Topics in Solid State Physics, vol.III* (North-Holland, Amsterdam, 1966).
215. T. R. McGuire and R. I. Potter, IEEE Transactions on Magnetics **11**, 1018 (1975).
216. P. J. Durham, B. L. Gyorffy, and A. J. Pindor, J. Phys. F: Met. Phys. **10**, 661 (1980).
217. J. Banhart, H. Ebert, P. Weinberger, and J. Voitländer, Phys. Rev. B **50**, 2104 (1994).
218. S. U. Jen, Phys. Rev. B **45**, 9819 (1992).
219. S. Senoussi, I. A. Campbell, and A. Fert, Solid State Commun. **21**, 269 (1977).
220. A. Hamzić, S. Senoussi, I. A. Campbell, and A. Fert, J. Phys. F: Met. Phys. **8**, 1947 (1978).
221. S. U. Jen, T. P. Chen, and B. L. Chao, Phys. Rev. B **48**, 12789 (1993).
222. T. R. McGuire, J. A. Aboaf, and E. Klokholm, J. Appl. Physics **55**, 1951 (1984).
223. J. Banhart, A. Vernes, and H. Ebert, Solid State Commun. **98**, 129 (1996).
224. F. P. Beitel and E. M. Pugh, Phys. Rev. **112**, 1516 (1958).
225. P. P. Freitas and L. Berger, Phys. Rev. B **37**, 6079 (1988).
226. J. Smit, Physica **16**, 612 (1951).
227. O. Jaoul, I. A. Campbell, and A. Fert, J. Magn. Magn. Materials **5**, 23 (1977).
228. W. H. Butler, X. G. Zhang, D. M. C. Nicholson, and J. M. MacLaren, J. Magn. Magn. Materials **151**, 354 (1995).
229. P. Weinberger *et al.*, J. Phys.: Condensed Matter **8**, 7677 (1996).
230. J. Banhart, private communication, 1998.
231. T. Huhne and H. Ebert, Solid State Commun. to be submitted (1998).
232. W. Geerts *et al.*, Phys. Rev. B **50**, 12581 (1994).
233. H. Ebert *et al.*, Mat. Res. Soc. Symp. Proc. **475**, 407 (1998).
234. Y. Suzuki, T. Katayama, P. B. S. Yuasa, and E. Tamura, Phys. Rev. Letters **80**, 5200 (1998).
235. M. Faraday, Phil. Trans. Roy. Soc. **136**, 1 (1846).
236. H. R. Hulm, Proc. Roy. Soc. (London) A **135**, 237 (1932).
237. J. L. Erskine and E. A. Stern, Phys. Rev. B **12**, 5016 (1975).
238. G. Schütz *et al.*, Phys. Rev. Letters **62**, 2620 (1989).
239. R. Wienke, G. Schütz, and H. Ebert, J. Appl. Physics **69**, 6147 (1991).
240. B. T. Thole, P. Carra, F. Sette, and G. van der Laan, Phys. Rev. Letters **68**, 1943 (1992).
241. G. Schütz, M. Knülle, and H. Ebert, Physica Scripta **T49**, 302 (1993).
242. P. Carra, B. T. Thole, M. Altarelli, and X. Wang, Phys. Rev. Letters **70**, 694 (1993).

243. H. Maruyama *et al.*, J. Magn. Magn. Materials **104**, 2055 (1992).
244. H. Ebert *et al.*, Int. J. Mod. Phys. B **7**, 750 (1993).
245. H. Ebert and H. Akai, Int. J. Mod. Phys. B **7**, 922 (1993).
246. F. Baudelet *et al.*, J. Phys. (Paris) **7**, C2 441 (1997).
247. S. Stähler *et al.*, J. Appl. Physics **73**, 6063 (1993).
248. J. Mustre de Leon *et al.*, Phys. Rev. B **44**, 4146 (1991).
249. D. O. Ahlers, Ph.D. thesis, Universität Würzburg, 1998.
250. V. Popescu, H. Ebert, and A. C. Jenkins, J. Synchr. Rad. **5**, in press (1998).
251. P. J. Feibelman and D. E. Eastman, Phys. Rev. B **10**, 4932 (1974).
252. B. Ackermann and R. Feder, J. Phys. C: Solid State Phys. **18**, 1093 (1985).
253. B. Ginatempo, P. J. Durham, B. L. Gyorffy, and W. M. Temmerman, Phys. Rev. Letters **54**, 1581 (1985).
254. P. J. Durham, in *The Electronic Structure of Complex Systems*, edited by P. Phariseau and W. M. Temmerman (Plenum Press, New York, 1984), p. 709.
255. P. J. Durham, J. Phys. F: Met. Phys. **11**, 2475 (1981).
256. H. Ebert and G. Y. Guo, J. Magn. Magn. Materials **148**, 174 (1995).
257. H. Winter, P. J. Durham, and G. M. Stocks, J. Phys. F: Met. Phys. **14**, 1047 (1984).
258. P. Marksteiner *et al.*, Phys. Rev. B **34**, 6730 (1986).
259. D. Weller and W. Reim, Appl. Physics A **49**, 599 (1989).
260. M. Schröder *et al.*, Phys. Rev. B **52**, 188 (1995).
261. S. Ostanin and H. Ebert, Phys. Rev. B **58**, 11577 (1998).
262. D. Weller *et al.*, Mater. Res. Soc **313**, 501 (1993).